Single mode Holey Fiber in GeGaSbS chalcogenide glass

Brilland Laurent, Nicholas Traynor , Achille Monteville
PERFOS (Plateforme d'études et de Recherche sur les Fibres Optiques Spéciales) ; 11 rue Louis de Broglie 22300 Lannion, France,
lbrilland@perfos.com

Frederic Smektala, Johan Troles
Laboratoire Verres et Céramiques ;UMR CNRS 6512CampusBeaulieu, Avenue du Général Leclerc 35042 Rennes Cedex France
frederic.smektala@univ-rennes1.fr)

Thierry Chartier, Thanh Nam Nguyen
Laboratoire d'Optronique de l'ENSSAT ; UMR CNRS FOTON 6082 , 6 rue de Kérampont ; BP 80518 22305 Lannion Cedex France

Abstract: *We present recent results on the fabrication of a single mode Holey Fiber in GeGaSbS chalcogenide glass using the "Stack&Draw" technique. We measure a Mode Field Diameter of 8,3 µm and we estimate at 200 $W^{-1}km^{-1}$ the γ value.*

1. Introduction

Considerable interest lies in the development of nonlinear optical fibers for applications such as all optical regeneration, optical demultiplexing, raman amplification, wavelength conversion and broad band spectrum generation. The parameter $\gamma=2\pi n_2/\lambda A_{eff}$ is a measure of the fiber nonlinearity where λ is the wavelength, n_2 the nonlinear refractive index and A_{eff} the effective mode area. For standard single mode silica fiber (SMF), $n_2 \approx 2.2x10^{-20}$ m^2/W and $\gamma \approx 1$ $W^{-1}km^{-1}$ at 1550 nm. It is possible to significantly increase the nonlinear parameter by using materials with greater intrinsic nonlinearity and/or by reducing the effective mode area.
In chalcogenide glasses, n_2 has been measured to be between 100 to 1000 times larger than for silica glass. These glasses present a large wavelength transparency window (from about 1µm to about 10 µm) and a high refractive index (greater than 2). There are numerous chalcogenide compounds such as As_2S_3, As_2Se_3, GLS, $GeSe_4$, GaGeSbS which are attractive for nonlinear devices [1],[2] and which offer varying degrees of difficulty in the fabrication of single mode fiber (difficulties normally due to viscosity differences of core/clad glasses and crystallisation effects).
Nonlinear effects can be also enhanced by using holey fibers (HF). They are a new class of optical fibers first demonstrated at the end of the 90's [3] which consist of a periodic lattice of holes arranged around a solid core that run along the fiber length. Usually fabricated using silica glass, the holes are arranged on a hexagonal lattice, diminishing the effective refractive index in the cladding region giving rise to index guiding in the core. The remarkable optical properties exhibited by these structures are now well known: very small or very large mode areas; widely tuneable dispersion, with positive dispersion at short wavelengths; endlessly single mode operation. In silica glass, the most common fabrication method is the "Stack&Draw" technique. Glass capillaries are stacked in a hexagonal lattice of several rings, and surrounded by a glass jacket to form the fiber pre-form. This process enables the realisation of complex structures (incorporation of many rings, capillaries of varying size), is reproducible, and allows preservation of geometry from the pre-form through to the fiber. In the case of chalcogenide glass, there are few reports dealing with holey fibers and to our knowledge only the GLS glasses system has been treated, with very simple structures. [4],[5].
In this paper, we present recent results on the fabrication of a holey fiber with GaGeSbS chalcogenide glass using the "Stack&Draw" procedure. This represents, to the best of our knowledge, the first demonstration of a chalcogenide based holey fiber with the complex structure required (several rings of holes) to allow flexible dispersion tailoring.

2. Glass fabrication

The nominal composition is $Ga_5Ge_{20}Sb_{10}S_{65}$. High purity raw materials (5N) are used for glass fabrication. The elements are placed in sealed silica tube under vacuum (10-5 mb), and the batch is heated at 800°C for 12h. The glass transition temperature, Tg, is 305°C, the index of refraction is 2.25 at 1550nm and the nonlinear coefficient, n_2, is measured to be 120 times greater than that of silica. This particular glass is transparent from 0.6 µm to 10 µm (low loss fiber fabrication possible from 1 to 6 µm). This glass presents several advantages which make it an ideal

candidate for the "stack and draw" technique: shallow variation of viscosity with temperature allowing stable fiber draw over a range of several tens of °C; absence of crystallisation effects around T_g.
To make the core rod, the glass is quenched in water and then annealed near the glass transition temperature for 30 min and cooled down to room temperature. For tube fabrication, a glass melt at 700°C is spun at 3000 rpm at ambient temperature during several minutes. During cooling, the viscosity increases and after a few minutes the vitrified tube is formed. The tube size used here is typically 12 cm*12mm*5mm (length*outer diameter*inner diameter).

3. Holey Fiber fabrication

A chalcogenide tube, placed in a suitable furnace in a drawing tower was drawn down to form capillaries with an outer diameter of 665 µm. These tubes were stacked in a three ring hexagonal lattice, with a rod of identical diameter in the central region, and placed in a larger jacket tube to create the pre-form. The jacket tube is collapsed around the micro-structure via an initial rapid descent through the furnace of the drawing tower, with very little deformation of the capillary tubes.
The fiber was then drawn at a rate of 5 m/min at a temperature of 540 °C. A variable pressure system enabled precise control of hole size during the draw.

4. Results

Figures 1 shows the cross section of the chalcogenide holey fiber. The outer diameter is 147µm, the distance between holes is Λ=8 µm and their diameter is about d=3.2 µm. In the upper right region the holes are larger than in the other regions. This is almost certainly due to the pre-form being off centre in the furnace, creating non uniform viscosity. The higher temperature region experiences lower viscosity and presents less resistance to the pressure inside the capillaries/holes.

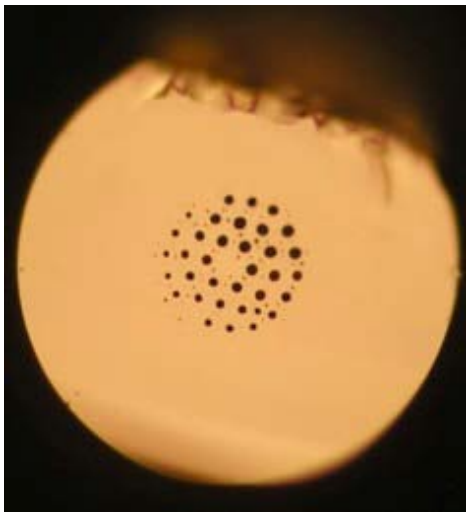

Figure 1: Transversal section of chalcogenide Holey Fiber

The output profile of guided modes at 1550 nm was investigated using a near field measurement. An indium metal coating was applied to inhibit cladding modes guidance. Light from a broadband source at 1550 nm was injected into the chalcogenide HF via a standard single mode fiberand the output form the fiber end was imaged onto an infrared camera. Figure 2 indicates single mode guiding with a Gaussian shape. The value of the ratio d/ Λ is estimated at 0,4. In reference [6], such a ratio indicates endlessly single mode operation for a HF with an index of refraction of 2.5.

The mode field diameter (MFD) at $1/e^2$ of maximum intensity was measured to be 8,3 µm, comparable to the MFD of conventional single mode fiber. The nonlinear parameter can be then estimated at $\gamma \approx 200 W^{-1}.km^{-1}$.

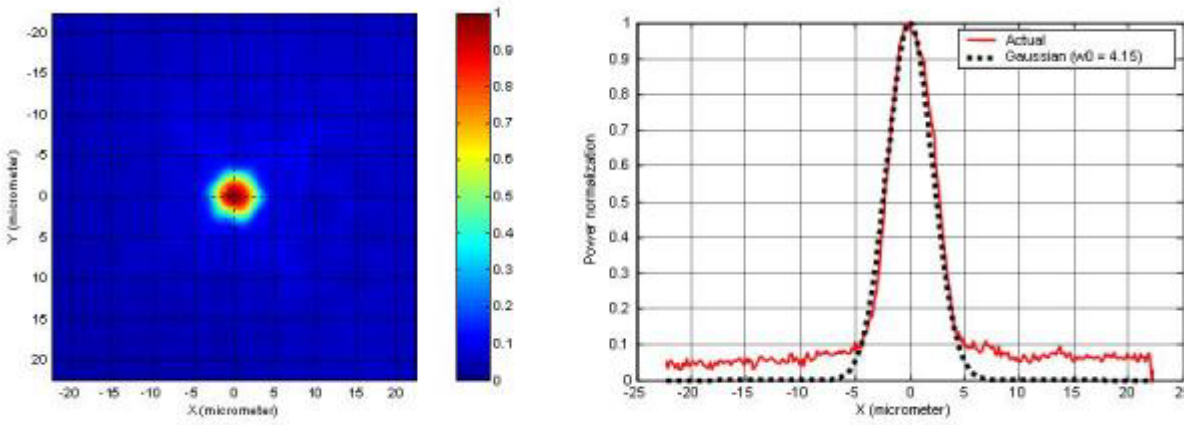

Figure 2: Experimental Mode Field Diameter measurement

Attenuation was measured, using a standard cut-back technique, to be 15 dB/m at 1550nm. This high value is probably due to a problem of pollution during the capillary drawing process. It is well known that loss in holey fibres is strongly dependent on surface quality and we have seen surface crystallisation on the outer and inner walls of capillaries supporting this hypothesis. The intrinsic optical loss at 1550 nm for this glass is 1.5 dB/m, allowing us to believe that a major improvement in fiber loss is possible.

5. Discussion and conclusion

We have demonstrated the possibility of fabrication of GaGeSbS chalcogenide Holey fiber using the "Stack&Draw" technique, with the realisation a single mode fiber with a MFD of 8.3 µm. We believe that the combination of this technique and chalcogenide glass holds great potential for the realisation of both small and large effective area fibers, with applications not only around 1550 nm but also in the mid infrared window. In silica single mode Holey Fiber, by stacking capillaries an A_{eff} of 1.3 μm^2 has been achieved [7]. For the chalcogenide Holey Fiber, strong glass/air index contrast will allow the realisation of extremely small effective areas making non linear coefficients in excess of 3000 $W^{-1}km^{-1}$ a realistic target. With further improvement of glass purifying methods and elimination of contamination during fabrication we believe that losses lower than 1dB/m can be achieved.

6. References

[1] J. Troles, F. Smekatala, G.Boudebs, A.Monteil, B.Bureau, J.Lucas, "Chalcogenide glasses as solid state optical limiters at 1.064µm", Optical materials 25 (2204) 231-237

[2] J. Sanghera, R.E. Slusher *et al*, "Large Raman gain and nonlinear phase shifts in high purity As_2Se_3 chalcogenide fibers", J. Opt. Soc. Am. B, Vol. 21, No. 6, 2004, pp. 1146-1155

[3] T.A. Birks, P.J. Roberts, P.St.J.Russel, D.M.Atkin, T.J.Sheperd, Electron. Lett. 31 (1995) 1941.

[4] T.M. Monro et al,"Chalcogenide Holey Fibres", Elect. Let., Vol.36, No24, 2000, pp. 1998-2000.

[5] D. W.Hewak et al, "The fabrication and modelling of non silica microstructured optical fibres" Optical Fiber Conference 2001.

[6] F. Bordas, L. Provino, G. Renversez, "Fibres optiques microstructures de haut indice: pertes et dispersion chromatique du fundamental et cutoff du second mode, comparaison avec la silice" Journees Nationales d'Optique Guidée,2004

[7] T.Monro at al, «Highly nonlinear holey fibers: design, manufacture and device applications", ECOC 2002

7. Acknowledgement

We thank Georges Boudebs and Sudir Cherukulappurath from POMA Laboratory, Angers University France, for n_2 measurement

Improvement of the Local Error Split-Step Fourier Method to Solve the Nonlinear Schrödinger Equation

T. N. Nguyen, T. Chartier
UMR CNRS 6082 FOTON, ENSSAT, 6 rue de Kerampont, 22300 Lannion, France
nguyen@enssat.fr

Abstract

We review some of the split-step Fourier methods to solve the nonlinear Schrödinger equation. An improvement of the local error method in the procedure of computation is proposed. The numerical simulations show that our method is more efficient than the original method. Our method is successfully applied to fit the experimental results of higher-order soliton compression in a highly nonlinear holey fiber.

1 Introduction

Pulse propagation in an optical fiber is governed by the nonlinear Schrödinger equation [1] (NLSE). The split-step Fourier method (SSFM) is one of the most efficient numerical method to solve the NLSE. Since its first use by Hasegawa [2], it has been applied world-wide in many issues such as wave propagation, graded-index fibers, semiconductor lasers, waveguide couplers. To improve the efficiency and the accuracy of the SSFM, one has developed some methods such as the higher-order SSFM [3], the multi-step SSFM [4] or the variable step-size Fourier methods [5]. To improve the efficiency of SSFMs, one often make a combination of these methods to get a hybrid-SSFM.

Generally, the variable step-size Fourier methods are system-dependent, i.e. one must know some of the characteristics of the system. Recently, Sinkin *et al.* [5] have proposed the variable step-size local error method (LEM) and Rieznik *et al.* [6] have proposed the variable step-size uncertain principle method (UPM). Both methods have the advantage to work without knowing any characteristics of the system. In contrast with the LEM, the UPM is more efficient for global errors δ_g from 10^{-3} to 10^{-1} (low accuracy) but less efficient for global errors δ_g less than 10^{-3} (high accuracy). Furthermore, the UPM has the disadvantage that, in some particular cases, the method may not ensure point-to-point convergence [6]. The LEM shows its powerful performance over other methods. However the main impairment of this method is a significant computational time for low accuracy results [5].

In this paper we propose an improvement of the LEM method to decrease the simulation processing time. The paper is organized as follows. Section 2 recalls the nonlinear Schrödinger equation. The basics of split-step Fourier methods are presented in section 3. In section 4, the LEM is presented in details. In Section 5 we present our approach to improve the LEM. Finally, section 6 gives an example of simulation using our method for high-order soliton pulse compression experiment.

2 The nonlinear Schrödinger equation

The NLSE is a nonlinear partial differential equation that governs many physical phenomena. Wave propagation is one of these phenomena. It is described, in a lossless optical fiber, as following [1]:

$$\frac{\partial U}{\partial z} + \frac{i}{2}\beta_2 \frac{\partial^2 U}{\partial \tau^2} - i\gamma |U|^2 U = 0, \tag{1}$$

where $U(z, \tau)$ is the normalized slowly-varying envelope of the electric field, z the propagation distance, τ the time (in a frame of reference moving with the pulse at the group velocity), β_2 the second-order group-velocity dispersion (GVD) parameter ($\beta_2 < 0$ in anomalous dispersion regime) and γ the nonlinear coefficient (optical Kerr effect).

3 Description of the split-step Fourier method

It is convenient to rewrite equation (1) as :

$$i\frac{\partial U}{\partial z} = (\mathbf{L} + \mathbf{N})U \tag{2}$$

where $\mathbf{L}$ is the linear operator and $\mathbf{N}$ the nonlinear operator, defined as :

$$\mathbf{L} = -\frac{i}{2}\beta_2 \frac{\partial^2}{\partial \tau^2} \tag{3}$$

$$\mathbf{N} = i\gamma |U|^2 \tag{4}$$

The solution of equation (2) can be found by assuming propagation over a small distance h and considering that $\mathbf{N}$ is quasi unchanged after propagation over h:

$$U(z + h, \tau) \approx e^{h(\mathbf{L}+\mathbf{N})} U(z, \tau) \tag{5}$$

In some special cases, relation (5) is also the exact solution if $\mathbf{N}$ is z-independent.

To consider propagation over a long distance, one divides the fiber into many small steps and applies the solution given by equation (5) on each step. This gives the numerical solution of the NLSE. This method is called the split-step method.

Now, the problem turns out to solve equation (5). In literature, to our best knowledge, three methods were proposed : the finite-difference method, the Fourier method and the spline method. Tara *et al.* pointed out that the Fourier method is more efficient than the finite-difference method thanks to the implementation of the fast Fourier transform (FFT) algorithm [7]. The spline method has just been proposed since 2004 [8] and has not been much attracted yet. Therefore, the Fourier method has dominated in many simulations of optical transmission systems [1].

The combination of split-step and Fourier methods to solve equation (1) is called the split-step Fourier method (SSFM). Several SSFMs can be implemented depending on the order of approximation of the right-hand side of equation (5) and on the way to choose the splitting step size. The simplest SSFM is the first order split-step method with constant step-size.

To estimate the accuracy of SSFM, it is useful to recall the Baker-Hausdorff formula [9] for any operators $\mathbf{L}$ and $\mathbf{N}$:

$$e^{\mathbf{L}} e^{\mathbf{N}} = e^{\left(\mathbf{L}+\mathbf{N}+\frac{1}{2!}[\mathbf{L},\mathbf{N}]+\frac{1}{3!}\{[\mathbf{L},[\mathbf{L},\mathbf{N}]]+[[\mathbf{L},\mathbf{N}],\mathbf{N}]\}+\ldots\right)} \tag{6}$$

where $[\mathbf{L}, \mathbf{N}] = \mathbf{LN} - \mathbf{NL}$ is the commutator of $\mathbf{L}$ and $\mathbf{N}$.

This equation is used to approximate the right-hand side of equation (5). For first order SSFM, only first-order terms are taken in the right-hand side of equation (6). Then, equation (5) becomes :

$$U(z+h,\tau) \approx e^{h\mathbf{L}} e^{h\mathbf{N}} U(z,\tau), \tag{7}$$

The error introduced by using the first-order approximation can be associated to the second-order term : $h^2[\mathbf{L},\mathbf{N}]/2$.

To solve equation (7), one needs to solve two sub-equations consecutively :

$$U'(z+h,\tau) = e^{h\mathbf{N}} U(z,\tau), \tag{8}$$
$$U(z+h,\tau) = e^{h\mathbf{L}} U'(z+h,\tau). \tag{9}$$

Equation (8) can be solved straightforwardly because $\mathbf{N}$ is a multiplicative operator. With equation (9), the Fourier method should be applied because $\mathbf{L}$ is a differential operator. After transposing (9) in the frequency domain by mean of Fourier transform, $\mathbf{L}$ becomes a multiplicative operator. Finally, the solution of equation (5) can be written as:

$$U(z+h,\tau) \approx F^{-1}\left\{ e^{-ih(i\omega)^2\beta_2/2} F\left[e^{ih\gamma|U|^2} U(z,\tau)\right]\right\}, \tag{10}$$

where F denotes the Fourier-transform operation and F^{-1} the inverse Fourier transform.

Physically, it can be understood that a wave, propagating along the fiber, experiences the two interleaving effects including linear effect (i.e. GVD effect) and nonlinear effect (i.e. Kerr effect). In each small step, the first order SSFM considers that both effects act independently. The algorithm of first order SSFM is presented in figure 1.

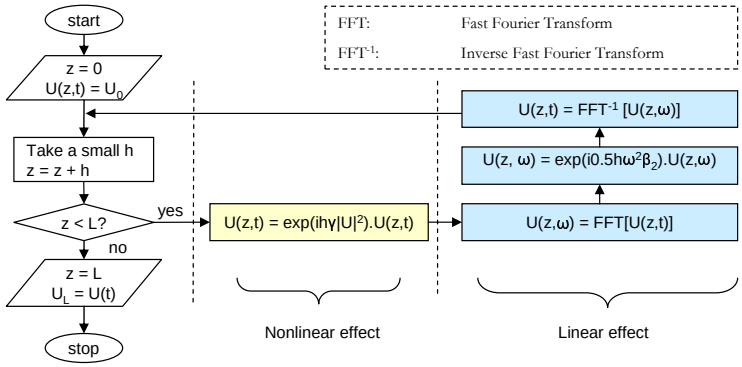

Figure 1: Algorithm of first order split-step Fourier method.

To improve the accuracy of the SSFM, one should add higher-order terms in equation (6). It is not very surprising that the higher the order of splitting approximation is, the more accurate the solution is. However, the simplicity of computational algorithm is sacrificed and the computational time is increased. This paper is limited to the second-order SSFM. Reader can find further description to higher-order SSFM in Ref. [3].

The second order SSFM is presented as the form [1, 3]:

$$U(z+h,\tau) \approx e^{\frac{h}{2}L} e^{hN} e^{\frac{h}{2}L} U(z,\tau), \tag{11}$$

This equation is symmetric and is known as the symmetrized split-step Fourier method (S-SSFM). Its solution is accurate to the third order in the step-size h[1].

[1]In fact, to calculate the error of S-SSFM method, one simply has to apply the equation (6) twice in

Physically, with the S-SSFM, an optical pulse experiences both the linear effect and the nonlinear effect but the nonlinear effect is lumped in the middle of the step while the linear effect impacts in each half-step.

4 System-independent local error split-step Fourier method

The aim of the local error method (LEM) is to provide a scheme to select the optimal step size for all kinds of systems. The basic principle is to ensure that the local error (error in each single step) is bounded by a certain value δ_G (the goal local error). It allows up to one more order of accuracy in comparison with constant step-size methods. The algorithm of this method applied to S-SSFM is described as following.

Step 1. Carry out the calculation of S-SSFM for $U(z,\tau)$ with a step size of $2h$ to find the solution at $z+2h$, called the coarse solution U_c. Then rewrite U_c as $U_c = U_t(z+2h,\tau) + C(2h)^3 + O(h^4)$, where $U_t(z+2h,\tau)$ is the true solution at $z+2h$ and C a constant.

Step 2. Carry out the calculation of S-SSFM for $U(z,\tau)$ with two steps of size h to find the solution at $z+2h$, called the fine solution U_f. Similar to Step 1, rewrite U_f as $U_f = U_t(z+2h,\tau) + 2Ch^3 + O(h^4)$.

Step 3. Perform the estimation of the relative local error defined by

$$\delta = \frac{||U_f - U_c||}{||U_f||}, \tag{12}$$

where $||U|| = \sqrt{\int |U(\tau)|^2 d\tau}$.

Step 4. Find the optimal solution at $z+2h$:

$$U(z+2h,\tau) = \frac{4}{3}U_f - \frac{1}{3}U_c = U_t(z+2h,\tau) + O(h^4) \tag{13}$$

Step 5. Compare δ with δ_G to find the next step size :

- If $\delta > 2\delta_G$ then discard the solution in Step 4 and recalculate with the halved step size.
- If $\delta_G < \delta \leq 2\delta_G$ then the step size is divided by a factor of $2^{1/3}$ for the next step.
- If $\delta_G/2 < \delta \leq \delta_G$ then the step size is the same for the next step.
- If $\delta \leq \delta_G/2$ the step size is multiplied by a factor of $2^{1/3}$ for the next step.

The aim of this procedure is to ensure that the local error in each step is kept in the range $(1/2\delta_G, \delta_G)$.

5 Improvement of the local error method

Analyzing the procedure of computation of the LEM, we found that it leads to a flexible step-size but that the distribution of the step-sizes along the transmission distance is not continuous but step-like. Furthermore, the algorithm leads to the calculation of many waste steps when somehow the step-size is too large.

We propose a modification to this procedure leading to a continuous distribution of step-size along the transmission distance. Besides, it avoids the calculation of many waste steps. This leads to a more efficient and more robust method. The most important point

---

the equation (11) :

$U(z+h,\tau) \approx \exp(\frac{h}{2}\mathbf{L})\exp(h\mathbf{N})\exp(\frac{h}{2}\mathbf{L})U(z,\tau) = \exp(\frac{h}{2}\mathbf{L})\exp(h\mathbf{N} + \frac{h}{2}\mathbf{L} + \frac{h^2}{4}\mathbf{NL} - \frac{h^2}{4}\mathbf{LN} + O(h^3))U(z,\tau) = \exp(\frac{h}{2}\mathbf{L} + h\mathbf{N} + \frac{h}{2}\mathbf{L} + \frac{h^2}{4}\mathbf{NL} - \frac{h^2}{4}\mathbf{LN} + \frac{h^2}{4}\mathbf{LN} + \frac{h^2}{4}\mathbf{L}^2 - \frac{h^2}{4}\mathbf{NL} - \frac{h^2}{4}\mathbf{L}^2 + O(h^3))U(z,\tau) = \exp(h\mathbf{N} + h\mathbf{L} + O(h^3))U(z,\tau)$

is that, the larger the global error is, the more efficient our method is. The modification focuses on the selection of the step size in Step 5:

- If $\delta > 2\delta_G$ then discard the solution in Step 4 and recalculate with the new step size.
- If $\delta \leq 2\delta_G$ then take the new step size for the next step.
- The new step size is defined by multiplying the present step size by $(\delta/\delta_G)^{1/3}$.

This modified local error method (MLEM) ensures that the local error is centered in δ_G. It prevents from the additional task when the local error increases too far from $2\delta_G$ or decreases too far from $\delta_G/2$. Moreover, it reduces the number of choosing conditions for selecting the step size, leading to a reduction of the computation time.

Figure 2 demonstrates the improvement of the performance of the MLEM in comparison with the LEM. These results are obtained by simulating the transmission of a 10 ps-pulse in a 5 km single-mode fiber. The dispersion of the fiber is 17 ps/km/nm, the nonlinear coefficient is 1.3 $W^{-1}km^{-1}$ and the attenuation is 0.2 dB/km. The time window is 320 ps and the number of points 4096. To compare both methods we use the global relative error as defined in Ref. [5] :

$$\delta_g = \frac{||U_n - U_a||}{||U_a||}, \tag{14}$$

where U_a is either an analytical solution (when it exists) or a numerical solution obtained with very small step-sizes, i.e. with very high accuracy. In this paper, U_a was found by using the S-SSFM with a step-size of 5 cm. U_n is the numerical result when we apply the method under test.

To evaluate the time consumption, we consider the number of implemented FFT functions. Three cases are taken into account when we change the ratio between nonlinearity and dispersion. In all cases the number of FFT using the MLEM is lower than the LEM.

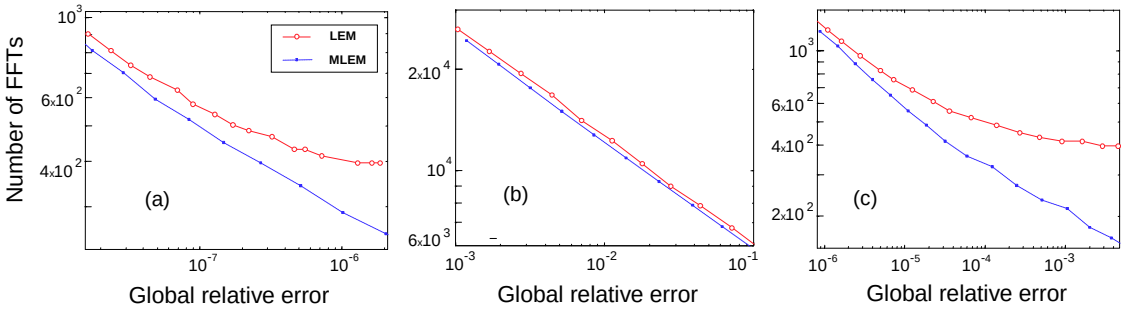

Figure 2: Comparison of the computational efficiency between LEM and MLEM for a 10 ps-pulse duration in a 5 km SMF fiber in three cases : the dispersion effect is dominant (a), the nonlinear effect is dominant (b) and both effects are comparable (c)

6 Modelling of a pulse compression experiment

We successfully use the MLEM to simulate higher-order soliton pulse compression in a 22 m-holey fiber. The principle is to launch a train of pulses of few ps in a fiber and then adjust the input power to obtain the adequate N-th order soliton evolution pattern [1]. This allows a maximum pulse compression at the output of the fiber. In our experiment, the nonlinear coefficient of the fiber is 26 $W^{-1}km^{-}1$, the dispersion is 120 ps/nm/km and the attenuation is 5 dB/km. The seed pulse is a secant hyperbolic pulse with a duration of 5.53 ps. The peak power is 0.69 mW. At the output of the fiber, we obtain a compressed pulse with a duration of 570 fs and with 71% of the energy in the central part of the pulse.

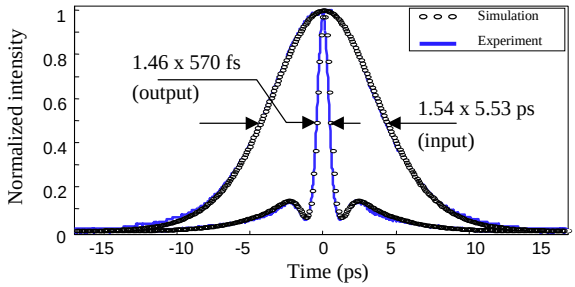

Figure 3: Autocorrelation traces of both simulation and experimental results in a pulse compression system.

Figure 3, represents the experimental results together with the result of simulation using the MLEM. This confirms the efficiency of the MLEM in modelling pulse propagation in a nonlinear and dispersive medium.

7 Conclusion

We have given a brief overview of the well-known split-step Fourier methods. From the user's point of view, some methods have simple algorithms but low accuracy while other methods provide better accuracy but with more complexity in algorithm and more computational time. We have proposed a modified local error method that reduces the computational time in solving the nonlinear Schrödinger equation with good accuracy and without knowing the characteristics of the system. The MLEM has been successfully used to simulate a higher-order pulse compression experiment in a highly nonlinear holey fiber.

Acknowledgements

This work is supported by the Conseil Régional de Bretagne (convention No.1193). Authors thank PERFOS (Lannion, France) for manufacturing the fiber used in the experiment and Mathilde Gay and Frédéric Ginovart (UMR FOTON, Lannion, France) for their comments on the manuscript.

References

[1] G. P. Agrawal, Nonlinear Fiber Optics, 2nd Ed., Academic Press, Inc. (1995).

[2] A. Hasegawa, Appl. Phys. Lett. **23**, p. 142 (1973) ; Appl. Phys. Lett. **23**, p. 171 (1973).

[3] G. M. Muslu, Math. Comput. Simul., In press.

[4] X. Liu, IEEE Photon. Technol. Lett. **15**, p. 1549 (2003).

[5] O. V. Sinkin, IEEE J. Lightwave Technol. **21**, p. 61 (2003).

[6] A. A. Rieznik, Opt. Exp. **13**, p. 3822 (2005).

[7] T. R. Tara, J. Comp. Phys. **55**, 203 (1984).

[8] M. Premaratne, IEEE Photon. Technol. Lett. **16**, p. 1304 (2004).

[9] G. H. Weiss, J. Math. Phys. **3**, p. 771 (1962).

Higher-order soliton-effect pulse compression in a non-linear holey fibre. Application to second-order dispersion measurement

T. N. Nguyen (1), T. Chartier (1), M. Thual (1), P. Besnard (1), L. Provino (2), A. Monteville (2), N. Traynor (2)
1 : UMR FOTON, ENSSAT, 6, rue de Kerampont, 22300 Lannion, France; chartier@enssat.fr
2 : PERFOS, 11 rue de Broglie, 22300 Lannion, France, ntraynor@perfos.com

Abstract *We report 570-fs pulse generation based on soliton-effect compression in a 22 m-long non-linear holey fibre. Using soliton-effect compression, we propose a simple method to measure second-order dispersion of fibres in the anomalous dispersion regime.*

Introduction

Since its first experimental demonstration [1], higher-order soliton effect pulse compression is a technique that has been widely used to generate ultrashort pulses in fibres [2]. Non-linear holey fibres (NLHF) are good candidates for this application because they allow reduction of both the required optical power and the fibre length [3]. In this communication, we report generation of 570 fs-pulses in a 22 m-long silica-based NLHF with an input optical power lower than 1 mW. In soliton-effect compression, both the compression factor and the quality of the compressed pulses depend on several parameters, in particular, the second-order group-velocity dispersion (GVD) of the fibre. We have derived an analytical relation that gives the value of the fibre GVD as a function of the non-linear coefficient, the fibre length, the input pulse width and the optical power required for optimum pulse compression. Using this relation, we propose a simple method for the measurement of positive GVD in fibres. This method has been successfully applied to different fibres in the anomalous dispersion regime.

Theory

Pulse evolution in a non-linear fibre is governed by GVD and self-phase modulation (SPM) [4]. In the anomalous dispersion regime, the soliton effect occurs as a result of a balance between GVD and SPM. While 1-st-order solitons preserve their shape during propagation, N-th-order solitons follow a periodic evolution pattern along the fibre such that they are periodically compressed [4]. The soliton order N is given by [4] :

$$N^2 = \frac{\gamma P_0 T_0^2}{|\beta_2|} \qquad (1)$$

where $\gamma = 2\pi n_2/\lambda_0 A_{eff}$ is the non-linear coefficient with n_2 the non-linear refractive index, λ_0 the wavelength in vacuum and A_{eff} the effective area. P_0 is the peak power of the pulse, T_0 the half-width (at 1/e-intensity point) of the pulse duration and β_2 the GVD parameter. The parameter β_2 is related to the other often-used dispersion parameter $D = -2\pi c\beta_2/\lambda_0^2$, where c is the speed of light in vacuum. By an appropriate choice of the fibre length z_c, input pulses can be compressed by a factor F_c. Quantities z_c and F_c depend on the soliton-order N and can be obtained by numerical simulations [1]. The optimum fibre length z_c can also be estimated from the following empirical relation [5]:

$$\frac{2z_c}{\pi L_D} = \frac{0.32}{N} + \frac{1.1}{N^2} \qquad (2)$$

where $L_D = T_0^2/|\beta_2|$ is the dispersion length. We can also interpret equation (2) as follows: for a given fibre length L, there exists a soliton number, N_c, that optimizes pulse compression at the fibre output. This soliton number N_c is obtained from the input peak power P_c. From equation (2), we have obtained the following relation:

$$D \approx \frac{2\pi c\gamma T_0^2 P_c}{\lambda_0^2 (2\gamma L P_c - 1.1\pi)^2} \qquad (3)$$

where we have assumed that $(0.32\pi)^2 \approx 1$. This relation gives this important result that, for a fibre of length L, if γ is known, the measurement of the peak power P_c for which the maximum soliton-compression is reached, gives access to the value of dispersion D.

Non-linear Fibre

The fibre used was a 5 rings NLHF fabricated by a standard stack and draw technique (figure 1). The measured non-linear effective area, A_{eff}, is 4.1 µm^2, leading to a non-linear coefficient γ = 26 W^{-1}km^{-1}. The optical losses, measured by an OTDR technique at 1550 nm, are 5.6 dB/km. The second order GVD, D, has been numerically evaluated (using a digitized image of the real fiber structure) to be 126 ps/km/nm at 1550 nm (figure 1).

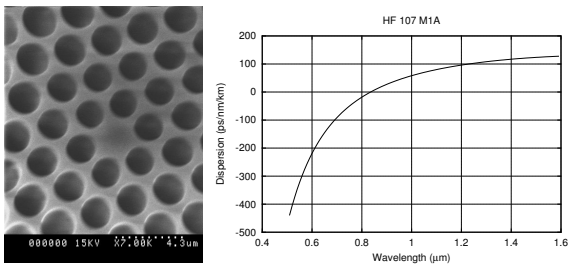

Fig 1: SEM photograph of the fibre core (left); calculated GVD versus wavelength (right).

Pulse compression

The experimental setup is shown in figure 2. The laser source is a passively-mode-locked fibre laser with the following characteristics : wavelength λ_0= 1560 nm, pulse duration T_0 = 3.14 ps (T_{FWHM} = 5.53 ps), spectral width $\Delta\lambda$ = 0.52 nm, repetition rate f = 19.3 MHz. The mean power launched in the NLHF is controlled with a power meter at the output of the 3 dB coupler. The total splicing loss between standard fibre (SMF 28) and NLHF is 1.2 dB.

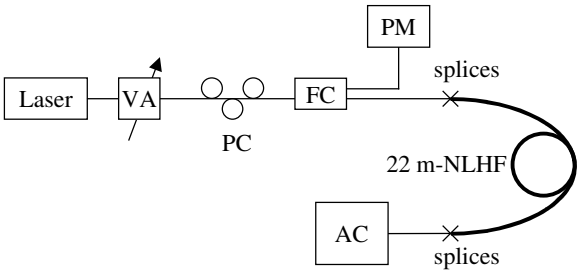

Fig. 2: Experimental set-up. VA : variable attenuator, PC : polarisation controller, FC : 3 dB fibre coupler, PM : powermeter, AC : Autocorrelator.

Results of pulse compression are shown in figure 3. For an averaged injected power $<P_c>$ = 0.69 mW, 570 fs-pulses can be obtained. For this value, the soliton order is $N \approx 3$ and the compression factor is F_c = 9.7. The quality factor Q_c, which is the ratio between the pulse energy contained in the central peak and the total pulse energy (including the wings of the pulse), has been estimated to 71 %. Higher compression factors could potentially be obtained with shorter fibre lengths and higher peak powers but with a degradation of Q_c [1].

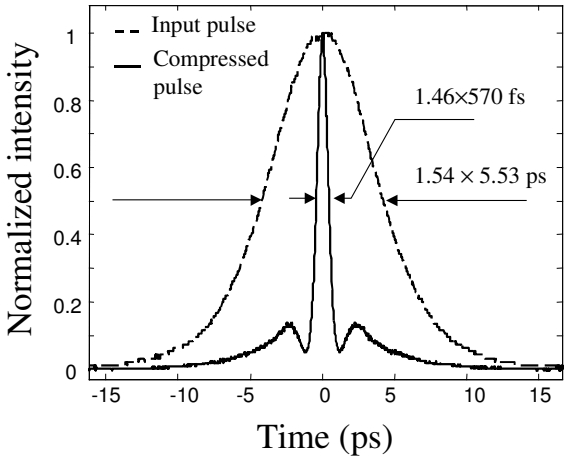

Fig. 3: Autocorrelation traces of both input pulses (dashed line) and compressed pulses (full line).

Dispersion measurement

Inserting the values of P_c, T_0, γ and L obtained from the previous experiment in Eq. (3), we find an experimental value of D equal to 120 ps/km/nm. This value is in good agreement with the numerical estimate (figure 1). In order to validate our dispersion measurement method, we have carried out additional experiments with different input pulse widths at different wavelengths and with two other fibres in the anomalous dispersion regime: a standard single-mode fibre (SMF) with D = 18.4 ps/km/nm at 1560 nm and a non-zero dispersion-shifted fibre (NZDSF) with D = 5.1 ps/km/nm at 1560 nm. Some of the results are summarised in table 1.

	L (m)	A_{eff} (μm^2)	γ ($W^{-1}km^{-1}$)	T_0 (ps)	$<P_c>$ (mW)	D (ps/km/nm)
NLHF	22	4.1	26	9.9	6.03	123
SMF	316	73	1.4	9.9	4.68	19.2
NZDSF	2050	52	2	9.9	0.38	5.2

Table 1: Results of dispersion measurements of NLHF, SMF, and NZDSF fibres at 1560 nm for T_0 = 9.9 ps (T_{FWHM} = 16.5 ps).

We note good agreement between our measured values and the real values of fibre GVD, indicating that our method is valid and reliable.

Conclusions

We have proposed a simple and rapid method to measure the second-order dispersion in optical fibres based on higher-order soliton-effect pulse compression. This method has been successfully applied to evaluate the dispersion of a 22 m-long non-linear holey fibre in a 570 fs- pulse generation experiment.

Acknowledgements

This work is supported by the Conseil Régional de Bretagne and the European Union (Fonds Européen de Développement Régional).

References

1 L. F. Mollenauer et al, Opt. Lett. **8** (1983), p. 289.
2 A. S. Gouveia-Neto et al, Opt. Lett. **12** (1987), p. 395.
3 J. H. V. Price et al, NLGW'01, Clearwater Florida (2001).
4 G. P. Agrawal, Nonlinear Fiber Optics, Academic Press, Inc. (1985).
5 E. M. Dianov et al, Sov. Tech. Phys. Lett. **12** (1986), p. 311.

Low Loss, Low OH, Highly Non-linear Holey Fiber for Raman Amplification

A. Monteville, D. Landais, O. LeGoffic, D. Tregoat, N.J. Traynor
PERFOS, 11 rue de Broglie, 22300 Lannion, France
ntraynor@perfos.com
T. N. Nguyen, S. Lobo, T. Chartier, J.-C. Simon
Laboratoire d'Optronique de l'ENSSAT ; UMR CNRS FOTON 6082, 6 rue de Kérampont, 22300 Lannion, France

Abstract: We present a highly non linear holey fiber with low loss and low OH absorption which enables us to demonstrate efficient Raman amplification in the C band with pump wavelengths of 1453 and 1480 nm.

OCIS codes: 060.2280, 060.2320, 060.4370

Micro-structured optical fibers (MOF) or holey fibers (HF) have found a plethora of applications since their first practical realization in 1996 [1]. While endlessly single mode fibers with mode field diameters close to those of standard fibers have been fabricated with losses approaching those of state of the art transmission fibers [2], very small core fibers, which benefit from the increased optical confinement afforded by a silica-air cladding, tend to exhibit losses which are significantly higher than their all-silica counterparts. These highly non-linear fibers benefit from the possibility to widely tune the chromatic dispersion and there are many reports of wideband supercontinua initiated by picosecond or nanosecond pulse sources operating close to the zero dispersion wavelength of the fiber. Such demonstrations require only a few meters of fiber and, as such, are generally insensitive to the magnitude of the fiber loss. Applications requiring longer lengths of non linear fiber such as Raman amplification [3] or supercontinuum generation using CW pump sources [4] have received much less attention, most likely due, in part, to the relatively high losses achieved in these fibers.

In this paper we present a low loss, non-linear HF which is particularly well suited to Raman amplification, especially in the 1,55 µm telecom window, due to an OH absorption peak at 1383 nm which is only limited by the intrinsic contamination levels of the raw silica materials used for fabrication. We also present, for the first time, results on Raman amplification in the C band using a highly non linear HF.

The fiber used was a 5 ring HF fabricated by a standard stack and draw technique (figure 1). We used F300 silica tubes and rods from Heraeus to make the capillaries and central rod for the micro-structured pre-form. This pre-form was then drawn down to a cane of 4 mm diameter and re-sleeved to a final diameter of 18mm, giving an outer diameter/core ratio for the final fiber of 125/2.5 µm. To achieve the lowest possible loss, and to avoid problems associated with OH contamination, the capillary tubes were chemically cleaned and finely polished. Pre-form preparation and fiber draw were made under controlled atmosphere conditions in order to avoid extrinsic contamination.

The optical losses of the fabricated fiber (figure 1), measured using both a cutback and an OTDR technique, were 6.9 dB/km at 1550 nm (5.6 dB/km with OTDR) and 38 dB/km at the water absorption peak (1383 nm). The difference between the two measurements at 1550 nm is most likely due to alignment errors of the very high NA fiber during cutback. The linearity of the OTDR trace indicates excellent homogeneity along the fiber.

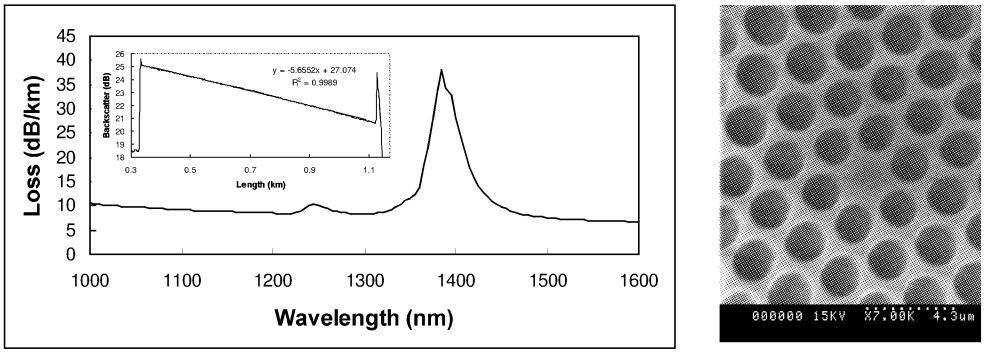

Figure 1: Measured fiber losses (left) by cutback and OTDR (inset). SEM photograph of the fiber core (right)

We believe these losses to be the lowest yet achieved for such a small effective area fiber (measured mode field diameter of 2.0 µm and measured non-linear effective area, Aeff, of 4.1µm^2). In particular, we have avoided the high Si-OH related losses generally found in small core HFs, which are often several 100s of dBs per km and at best around 75 dB/km[4]. Indeed, the observed OH peak (~30 dB/km of additional loss at 1385 nm) may well be material limited, as this corresponds to 0.6 ppm of OH concentration, within the specified levels for the raw materials [5].

We used 720m of this fiber in a standard Raman amplifier configuration. Two different pump sources were used in the experiments. Both were un-polarized Raman lasers with emission wavelengths of 1453 and 1480 nm respectively. These were injected into the HF via an appropriate WDM and a high numerical aperture intermediate fiber. The total splice loss (SMF to HF) was around 1.2 dB. The signal source (counter propagating) was a broadband source (signal input power: -20 dBm) for the 1453 nm pump and an external cavity laser diode at 1570 nm amplified by an EDFA (variable signal input power) for the 1480 nm pump.

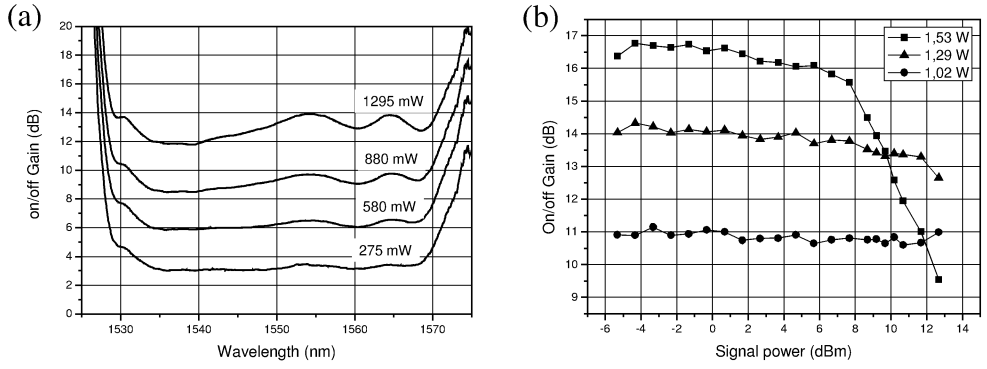

Figure 2 : On/off gains for (a) the 1453 nm pump source and (b) for the 1480 nm pump source

Figure 2a shows the on/off signal gain for the 1453 nm pump source. The indicated powers are launched pump powers in the HF. We obtain an on/off gain of 14 dB for 1.3 W of launched pump power. Figure 2b shows the on/off gain as a function of both input signal power and launched pump power for the 1480 nm pump. The maximum gain achieved was 17 dB for 1.5W of pump. At higher input signal power (+8 dBm) we observe the onset of strong Brillouin scattering which occurs for a signal output power of around +19 dBm. In both cases the observed gain was insensitive to the polarization state of the signal input. Using the measured values of gain, Aeff, fiber loss and pump power we are able to estimate the Raman gain coefficient, g, (non polarized pump) to be 2.5 ±0.2 m/W, which is in good agreement with previously measured values in HF [6], and indicates good confinement and overlap of the pump and signal modes. As can be seen the observed Raman gain values are insensitive to pump wavelength indicating that the OH absorption has little or no effect on Raman gain at 1453 nm.

The lumped amplifier gain (taking into account fiber loss) is around 12.5 dB for 1.5 W of pump power, or 8.3 dB/W. This gain value compares very favorably with previous experiments using small core holey fiber which achieved 6 dB/W with a polarized pump (equivalent to 3 dB/W un-polarized) and which used a Raman pump far from the water peak at 1536 nm [3].

In conclusion we have demonstrated the possibility to fabricate highly non-linear HF with low losses and OH contamination corresponding to the raw material intrinsic levels, and the subsequent utilization of these fibers in Raman amplification. With further efforts in surface treatment, and through the use of lower OH raw materials and Ge doped core rods, we believe that it will be possible to fabricate HFs with Raman gain efficiencies comparable to the best Ge doped fibers, which will facilitate extremely efficient Raman lasers and amplifiers, low power all-optical processing and CW pumped continuum generation.

Acknowledgements

The authors thank Monique Thual and Séverine Haesaert (CCLO, UMR FOTON, Lannion, France) for help in measurement of Aeff and SEM images, Laurent Bramerie (PERSYST, UMR FOTON, Lannion, France) for helpful discussions and access to PERSYST equipment. This work is supported by the Conseil Régional de Bretagne and the European Union (Fonds Européen de Développement Régional).

References

[1] J.C. Knight, T.A. Birks, P.St.J. Russell and D.M. Atkin, Opt. Lett., **21,** 1547-9 (1996).
[2] K. Tajima, J. Zhou, K. Kurokawa and K. Nakajima, ECOC'03 (Rimini, Italy), 42-43 (2003).
[3] Z.Yusoff, J.H.Lee, W.Belardi, T.M.Monro, P.C.Teh and D.J.Richardson, Opt. Lett., **27**, 424-6 (2002).
[4]J. C. Travers, R. E. Kennedy, S. V. Popov, J. R. Taylor, H. Sabert and B. Mangan, Opt. Lett. **30**, 1938-40 (2005).
[5] See specifications of F300 silica glass at www.heraeus-tenevo.com
[6] C. Fukai, K. Nakajima, J. Zhou, K. Tajima, K. Kurokawa and I. Sankawa, ECOC'04 (Stockholm, Sweden), 304-5 (2004).

Recent advances in the development of holey optical fibers based on sulfide glasses

F. Smektala[(1) *], L. Brilland[(2)], T. Chartier[(3)], T. N. Nguyen[(3)],
J. Troles[(1)], Y. F. Niu[(1)], S. Danto[(1)], N. Traynor[(2)], T. Jouan[(1)]

[(1)] UMR CNRS 6512 Verres et Céramiques, Institut de Chimie de Rennes, Université de Rennes 1, 35042 Rennes, France.
[(2)] Perfos, Plate-forme d'Etudes et de Recherches sur les Fibres Optiques Spéciales 11, rue Louis de Broglie, 22300 Lannion, France.
[(3)] Laboratoire d'optronique UMR CNRS 6082 Foton, ENSSAT, 6 rue de Kerampont, 22305 Lannion, France.

ABSTRACT

Microstructured optical fibers as new optical objects have been developed in the recent past years, firstly from silica glass and then from other oxide glasses such as tellurite or different heavy cations oxide glasses. However very few results have been reported concerning non-oxide glasses and more particularly chalcogenide glasses. In a photonic crystal fiber the arrangement of air holes along the transverse section of the fiber around a solid glassy core leads to unique optical properties, such as for example broadband single-mode guidance, adjustable dispersion, nonlinear properties. Since the effective modal area is adjustable thanks to geometrical parameters, chalcogenide microstructured fibers with small mode area are of interest for nonlinear components because of the intrinsic non linearity of chalcogenide glasses, several order of magnitude above these of the reference silica glass (100 to 1000 times the non linearity of silica glass). On the other hand, chalcogenide holey fibers with large mode area are of interest for infrared power transmission, in a wavelength range out of reach of silica fibers, and more particularly in the 3-5 µm atmospheric window. The aim of this paper is to present more specifically the recent results that have been achieved in the elaboration, light guidance and characterization of photonic crystal fibers from the sulfide $Ge_{20}Ga_5Sb_{10}S_{65}$ glass, which presents a large transparency window from 600 nm to 11 µm.

Keywords : Optical fibers, photonic crystal fibers, holey fibers**,** microstructured fibers**,** chalcogenide, sulfide, glasses.

1. INTRODUCTION

Chalcogenide glasses are well known for their broad transparency in the infrared wavelengths region, until 10 to 20 µm depending on their chemical composition. In the past recent years they have also been studied with regard to their non linear optical properties, especially these from the third order. Indeed, chalcogenide glasses are highly non linear, with non linear refractive indices n_2 between 2 and 20 10^{-18} m^2/W. These values represent around hundred to thousand times the n_2 of the reference silica glass (2.7 10^{-20} m^2/W @1064 nm) [1]. These remarkable optical properties make of these materials very interesting candidates to special optical applications such as Raman amplification, infrared super continuum generation, infrared laser power transmission, infrared chemical or biomedical sensors, infrared lasers when doped with rare earths and so on [2-7]. For these applications, the elaboration of single mode fibers is often necessary and single mode chalcogenide glass fibers in a step index configuration have been demonstrated through rod in tube or double crucible processes [8-9]. What's more, the recent development of photonic crystal fibers as new optical objects has

* Frederic.Smektala@univ-rennes1.fr; phone 33-2-23-23-56-20; fax 33-2-23-23-56-11; http://www.verceram.univ-rennes1.fr;

raised an enhanced interest for chalcogenide glass optical fibers. Indeed, microstructured optical fibers have been developed firstly from silica glass in the 1990's and then from other glasses such as tellurite or different heavy cations oxide glasses [10-11]. These fibers present a periodic arrangement of air holes along the transverse section of the waveguide around a solid core (holey fibers) or even around a central hole (photonic band gap fibers). However very few results have been reported concerning non-oxide glasses and more particularly chalcogenide glasses. Indeed, to our knowledge only the gallium lanthanum sulfide glass system has been treated and in the case of a very simple structure [12]. In this reference, a holey fiber is manufactured with only one ring of capillaries and presents an irregular profile. One of the great interests of microstructured fibers is that the mode field diameter (MFD) is widely adjustable : large MFDs are very useful to minimize the risks of glass damage during high power laser beams propagation when small MFDs enable the enhancement of nonlinear effects [13]. But other original optical properties are also achievable such as a widely tunable dispersion or an endlessly single mode operation for examples [14-15]. Thus, the development of photonic crystal fibers in the mid-infrared would be of great interest for laser power transmission in the 3-5 µm or even 8-12 µm atmospheric windows, infrared super continuum generation, and so on.

Then the aim of this paper is to present the recent achievements in the elaboration and characterization of microstructured optical fibers from the $Ge_{20}Ga_5Sb_{10}S_{65}$ sulfide glasses which present a large transparency window which extends from 600 nm in the visible to 11 µm in the infrared.

2. EXPERIMENTAL

2.1 Chalcogenide glasses synthesis and characterizations.

High purity raw materials (5N : 99,999%) are used for the preparation of the $Ga_5Ge_{20}Sb_{10}S_{65}$ (S2G2) glass [16]. However, sulfur is often polluted by water. It is then dehydrated by heating at 120°C under vacuum (10^{-5} mbar), before being distillated. The required amounts of the different elements are then placed in a silica ampoule which is sealed under vacuum (10^{-5} mbar) and progressively heated from room temperature to the refining temperature of 850°C at the heating rate of 2°C/min. This slow heating allows to obtain first the fusion of the gallium, the sulfur and then the antimony and their reaction with solid germanium and avoid a too fast volatilization of sulfur which would lead to the explosion of the ampoule. The batch is maintained at 850°C during10 hours, before being quenched in water at the cooling rate of approximately 100 K/s, to allow the glass formation and to avoid any crystallization process. After that, the vitreous sample is annealed for 1 hour at its glass temperature (Tg = 305°C) in order to relax the internal mechanical stress induced by the quenching, and is then slowly cooled to room temperature. [1; 17; 18]. The dimensions of the silica ampoule are typically 12 cm in length, and 12 mm in diameter. The quantity of glass is varying between 30 and 40g depending on the final shape of the sample, i.e. a glass rod or a glass tube. The bulk glass is transparent from 0.6 µm to 11 µm (figure 1). It presents a great stability against crystallization. Indeed, between 305 °C and 500°C, the DSC curve of this composition heated at a rate of 10°C/min exhibits no crystallization peak The linear refractive index of the glass is 2.250 at 1550 nm and the nonlinear refractive index n_2 is 3.2 10^{-18} m^2/W at 1064 nm from non linear imaging measurements [19-20]. This value corresponds to 120 times the non linearity of silica glass which is 2.7 10^{-20} m^2/W at 1064 nm [21]. At this wavelength, the non linear absorption coefficient of the 2S2G glass is equal to 0 cm/GW.

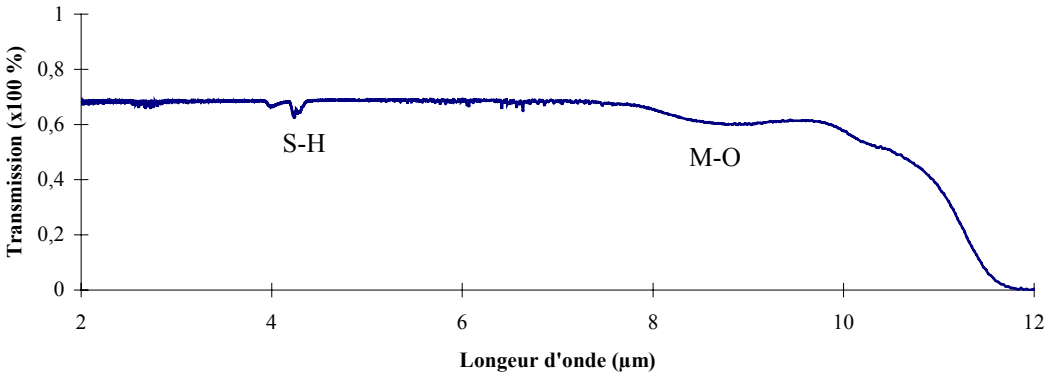

Figure 1 : Infrared transmission spectrum of S2G2 glass, thickness = 3 mm

2.2 Mono-index optical fibers elaboration and optical characterization.

In order to obtain a mono-index optical fiber from the S2G2 glass we stretch a glass rod on a drawing tower. For this purpose we firstly synthesize a glass rod with a diameter of typically 12 mm as described previously (paragraph 2.1). This rod is then fixed on the motion set up of the drawing tower (figure 2). The extremity of the rod is heated above Tg until the softening of the glass. A drop is formed which flow down under the effect of the gravity. The obtained fiber is then fixed on the drum which rotation allows the drawing of the glass rod [19; 22]. The diameter of the mono index optical fiber drawn by this way is controlled by the drum speed. It is typically 200 µm, but can varied from below 100 µm until several hundreds of microns. Several hundreds of meters of fiber are thus drawn. The fiber is then optically characterized by the cut back method with a the help of a FTIR spectrophotometer between 1.5 µm and 15 µm [23]. The typical attenuation curve of the S2G2 glass mono-index optical fibers is presented figure 3. The minimum of attenuation is 0.2 dB/m around 2.7 µm. Several extrinsic absorption bands are present, especially those associated with the S-H vibration which are due to a reaction between the glass and the remaining water in the batch.

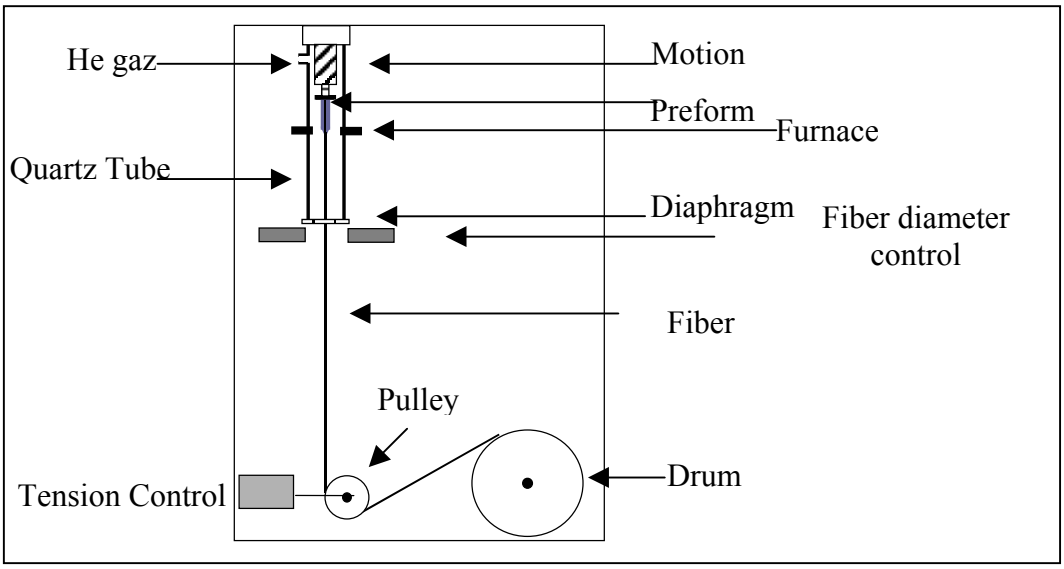

Figure 2 : Drawing tower.

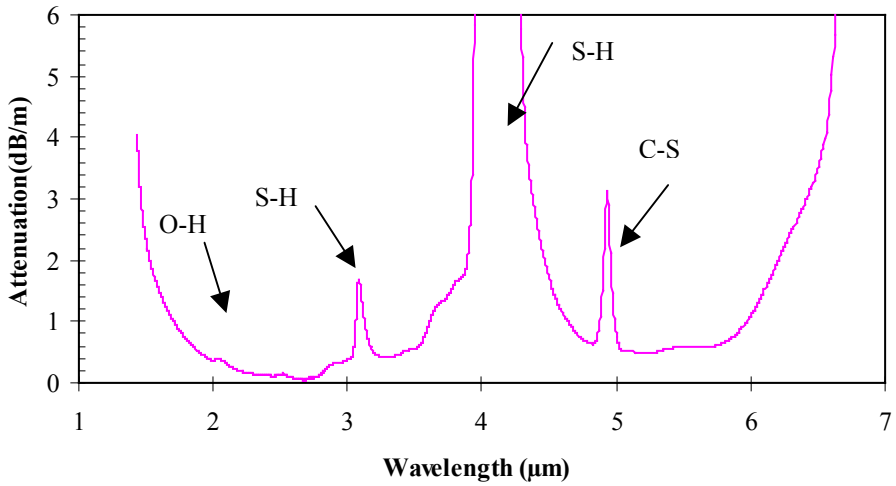

Figure 3 : Attenuation curve of a S2G2 glass mono-index optical fiber.

2.3 Holey fiber elaboration.

The elaboration of a holey optical fiber is realized through the stack and draw technique which consists to draw a preform presenting the required geometrical arrangement of air holes around a solid glassy core [24-25]. To obtain this preform, we stack an arrangement of glass capillaries in a hexagonal lattice of several rings around a central cylindrical core, this stack being jacketed by a glass tube. This stack and draw process enables the realisation of complex structures. Indeed, it is possible to stack many rings of capillaries. What's more, the capillaries can be of different sizes. The process is reproducible and allows preservation of the geometry during the drawing. It has been proved that several rings are necessary to seriously diminish guiding losses [26-27]. In the present paper, we report the elaboration of holey fibers from the S2G2 chalcogenide glass with structures based on three rings of holes. For the stack and draw process purpose, it is necessary to prepare a S2G2 glass rod and two S2G2 glass tubes as described previously (paragraph 2.1). The tubes are obtained by the rotational casting technique : the glass melt in its silica ampoule is carried at 700°C and then taken out the furnace and spun at 3000 rpm at room temperature in a stainless steel mould (figure 4a). During rotation, the cooling occurs, the viscosity increases and the formation of a vitreous tube is obtained after a few minutes (figure 4b). The tube size is typically 12cm x 12mm x 5mm (length x outer diameter x inner diameter).

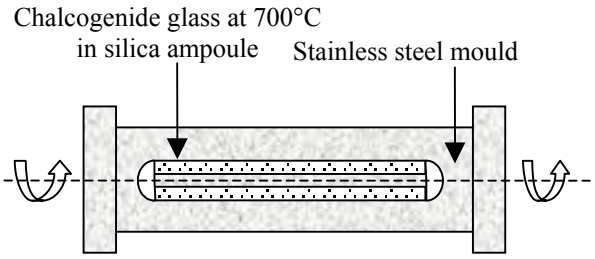

Figure 4a : Rotational casting set up

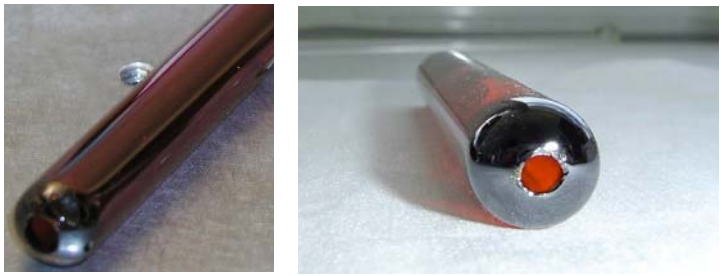

Figure 4b : Chalcogenide glass tubes obtained by rotational casting

The glass rod with an external diameter of 12 mm is stretched on the drawing tower to obtain a stick of typically 665 µm in diameter. A sample of 12 cm long is cut from this stick to serve as the core of the holey fiber. One of the glass tubes is also stretched on the drawing tower to an external diameter of 665 µm. The S2G2 glass capillaries of 12 cm long are then cut from this stretched tube and are stacked in hexagonal lattice around the core, in three different rings, corresponding to 36 capillaries. The stack is jacketed by the second glass tube (figure 5). The assembling is placed on the drawing tower and the external tube is collapsed on the stack by a fast translation through the hot furnace so that the glass reach a temperature around 100°C above Tg. These different steps lead to the elaboration of the preform. The S2G2 glass holey fiber is then drawn from this preform on the drawing tower at a speed of typically 5m/min and to an external diameter around 145 µm. A variable gas pressure set up enables precise control of hole size during the drawing.

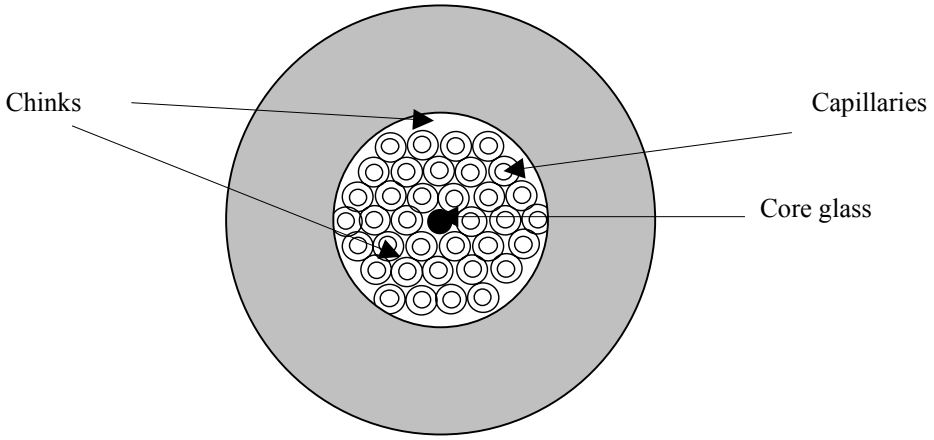

Figure 5 : Schematic view of an hexagonal stack of three rings of capillaries around a central core, surrounded by a jacketing tube.

3. RESULTS AND DISCUSSION

Several experiments have been conducted in order to achieve photonic crystal fibers from the sulfide S2G2 glass. Two of these attempts are presented in this paper and illustrates the improvements that have been achieved in the elaboration of sulfide glass holey fibers. The figure 6 presents two pictures of a holey fiber (HF 1) obtained from a hexagonal lattice constituted of three rings of capillaries around a solid core. The external diameter of fiber HF 1 is 145 µm. One picture came from an observation with a light microscope and the second from a scanning electronic microscope (SEM). One can observed from the pictures of the section of the fiber that more than 36 holes are present across the fiber. The external holes are also much larger than the other ones. The holes in excess came from the chinks existing between the capillaries when they are stacked (figure 5). The collapsing of the external tube was not sufficient in this case to fill them up in the jacketing step of the elaboration of the preform. For the same reason, the chinks present between the last ring of capillaries and the external tube were open. These chinks are the largest of the preform in this kind of stack (figure 5) and the gas pressure used during the drawing of the fiber leads preferably to their growth.

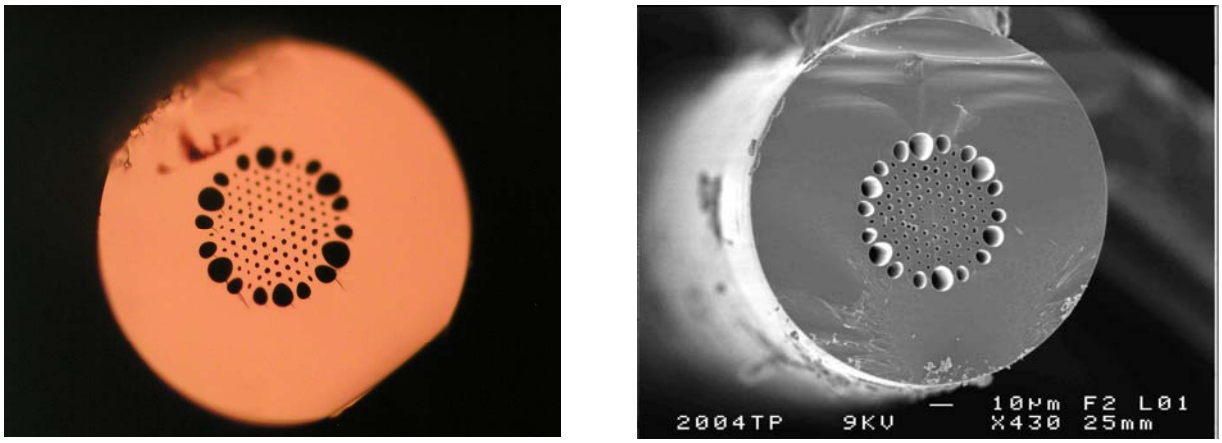

Figure 6 : Two pictures of the section of holey fiber HF 1.

The design of the preform of holey fiber HF 1 has been chosen so that the ratio d/Λ is equivalent to 0.42. In this parameter, d is the hole diameter and Λ is the pitch, corresponding to the distance between the centers of two adjacent holes. A holey fiber presenting a d/Λ parameter with $d/\Lambda \leq 0.42$ exhibits an endlessly single mode propagation behavior, and this whatever the refractive index of the glass [28]. Of course, in fiber HF 1 and because of the insufficient jacketing, the presence of holes in excess as well as the variability of holes diameters disrupt this parameter. However, the optical characterization of the fiber indicates a monomode operation. Indeed, the output profile of guided modes at 1550 nm are investigated using a near field measurement. Light from a broadband source at 1550 nm is injected into the S2G2 glass holey fiber HF 1 via a standard silica single mode fiber. An indium metal coating is applied on the surface of the HF 1 fiber to suppress cladding modes. The output beam of the HF1 fiber is then imaged onto an infrared camera (figure 7a). The figure 7b shows the accurate gaussian fit of this profile, indicating a monomode behavior. The mode field diameter (MFD) at $1/e^2$ of maximum intensity is measured to be 8.3 µm, comparable to the MFD of the conventional silica single mode fiber.

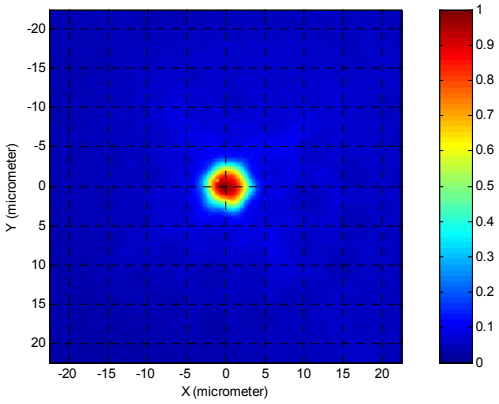

Figure 7a : Image of the output beam of HF1 fiber.

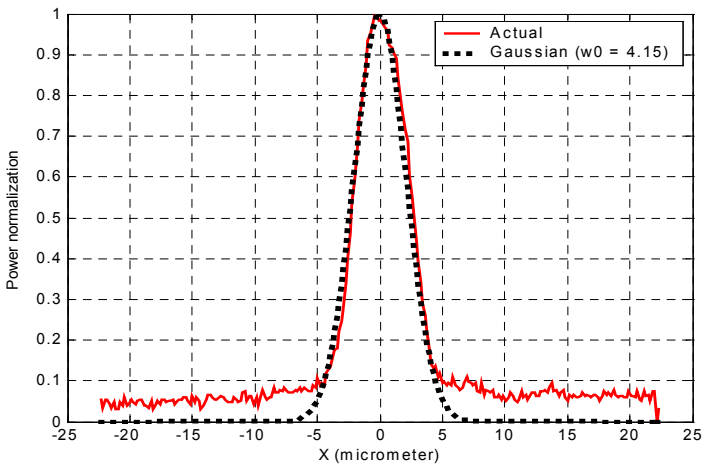

Figure 7b : Gaussian fit (doted line) of the output beam of HF1 fiber.

Another 3 rings Holey Fiber (HF 2) with an external l diameter of 137 µm has been elaborated under the same experimental conditions, but with a better control of the jacketing step, allowing a better collapse of the external tube on the stack of capillaries. The chinks are in this case almost completely filled. Just few of them are not totally closed as it can be seen on a light microscope picture (figure 8a). They are especially those situated at the circumference of the capillaries stack, between the third ring and the external jacketing tube, corresponding to the largest free spaces of the preform (figure 5). The pitch Λ is in this case 7.7 µm and the diameter of the holes d is 4,85 µm. The corresponding ratio d/ Λ is thus 0.63. This indicates a multimode guiding at 1550 nm even with only three rings of holes [28]. The holey fiber HF 2 is then characterized in the near field using the same procedure as described previously with only the excitation of the fundamental mode (figure 8b). Following a Gaussian approximation experimental measurements give the mode field diameter (MFD) at 9,3 µm on the x-axis and 9,66µm on the y-axis.

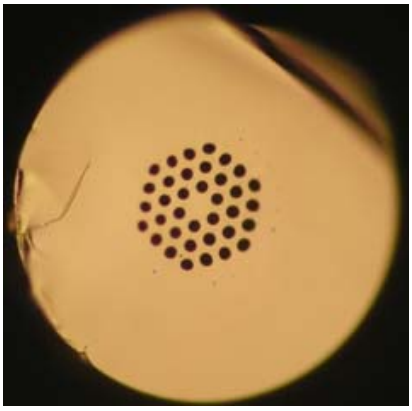

Figure 8a: Picture of the cross section of S2G2 glass holey fiber HF2.

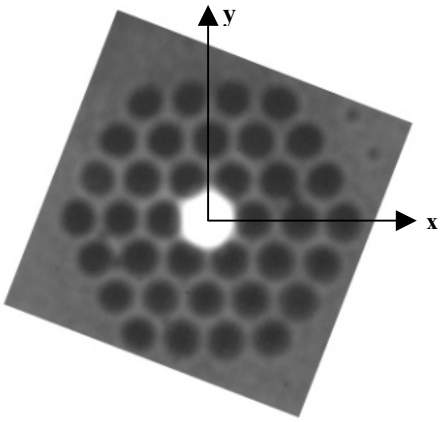

Figure 8b: Near field observation of the guided beam at 1.55µm in holey fiber HF 2.

In this work, we present the elaboration of two chalcogenide holey fibers presenting three rings of holes, one single mode and the second multimode. To the best of our knowledge, this work is the first demonstration of the stack and draw technique applied to the elaboration of a multi-layer index guiding holey fiber based on a sulfide

$Ge_{20}Ga_5Sb_{10}S_{65}$ glass. We have focused here on the manufacture of holey fibers with a mode field diameter near that of standard MFD of single mode silica fiber in order to facilitate the coupling with a SMF28 fiber.

We believe that this work can be developed to produce very small MFDs with only 3 or 4 rings of holes. Indeed, the high index of refraction of chalcogenide glasses enables a better confinement of the light. For example, a 4 rings holey fiber elaborated from a high index glass (n=2.5) with a parameter $d/\Lambda=0.4$ and a pitch $\Lambda=2.3$ µm, exhibits guiding losses below 5 dB/km at $\lambda=1550$nm as calculated from the multipole method [29]. These guiding losses are significantly lower than the actual 1-2 dB/m $Ga_5Ge_{20}Sb_{10}S_{65}$ fiber losses around 1550 nm (figure 3). Such a structure could be of significant interest for the realization of compact non linear devices, associated to the high intrinsic non linear refractive index of the S2G2 glass (120 times higher than that of silica glass).

On the other hand, this work can also be pursued towards the development of single mode holey fibers with large mode field diameters for power laser transmission in the atmospheric window between 3 and 5 µm, at the condition that the extrinsic S-H absorption band should be drastically reduced. Different attempts are actually in progress in these two directions.

4. CONCLUSION

Several holey fibers base on the $Ge_{20}Ga_5Sb_{10}S_{65}$ chalcogenide glass have been elaborated. We demonstrate the possibility of complex structures achievements, up to 3 rings of holes, using the stack and draw process. We believe that the combination of this technique with the remarkable linear and non linear optical properties of chalcogenide glasses holds great potential for the realization of both small and large effective area fibers, with applications not only around 1550 nm but also in the mid infrared window, up to 6 µm in the case of sulfide glasses. In future work, we plan to improve the purity of our chalcogenide glasses and our drawing process in order to reduce the overall losses.

ACKNOWLEDGEMENTS

Many thanks to Georges Boudebs, from the POMA Laboratory, UMR CNRS 6136, University of Angers in France for non linear measurements, and to Gilles Renversez from Institut Fresnel, UMR CNRS 6133, Université Paul Cézanne Aix-Marseille, Marseille in France, for theoretical calculations on chalcogenide holey fibers.

We acknowledge also the french DGA for its support through the grant : "Fibres microstructurées à base de verres de chalcogénures – Transport de faisceaux de puissance à guidage monomode entre 3 et 5 µm".

REFERENCES

1. F. Smektala, C. Quemard, V. Couderc, A. Barthelemy, "Non-linear optical properties of chalcogenide glasses measured by Z-scan ", J. of Non-Cryst. Solids, **274** (200) 232-237.
2. J. Troles, F. Smektala, G. Boudebs, A. Monteil, B. Bureau, J. Lucas, "Chalcogenide glasses as solid state optical limiters at 1.064µm", Opt. Mater. **25** (2004) 231-237.
3. J. Sanghera, R.E. Slusher, "Large Raman gain and nonlinear phase shifts in high purity As_2Se_3 chalcogenide fibers", J. Opt. Soc. Am. B, **21**, 6 (2004) 1146-1155.
4. K. Michel, B. Bureau, C. Boussard-Plédel, T. Jouan, J.L. Adam, K. Staubmann and T. Bauman, "Monitoring of pollutant in waste water by infrared spectroscopy using chalcogenide glass optical fibers", Sensors and Actuators B, **101**, 1-2 (2004) 252-259.
5. M.F. Churbanov, I.V. Scripachev, V.S. Shiryaev, V.G. Plotnichenko, S.V. Smetanin, E.B. Kryukova, Yu.N. Pyrkov, B.I. Glagan, "Chalcogenide glasses doped with Tb, Dy and Pr ions", J. of Non-Cryst. Solids **326&327** (2003) 301-305.
6. F. Smektala, K. Le Foulgoc, L. LeNeindre, C. Blanchetière, X. H. Zhang, J. Lucas, "TeX-Glass infrared optical fibers delivering medium power from a CO_2 laser", Opt. Mater. **13** 2 (1999) 271-6.
7. F. Smektala, B. Bureau, J.L. Adam, J. Lucas, "Infrared waveguides for applications in telecommunications and chemical or biochemical sensors", J. Phys IV **12** (2002) 41-51.

8. J. Nishii, T. Yamashita, T. Yamagishi, "Chalcogenide glass fiber with a core-cladding structure", Appl. Optics **28** (1989) 5122-6.
9. P. Houizot, F. Smektala, V. Couderc, J. Troles, L. Grossard, "Selenide glass single mode optical fiber for non linear optics", Opt Mater. to be published (2006).
10. T.A. Birks, P.J. Roberts, P.St.J. Russel, D.M. Atkin, T.J. Sheperd, "Full 2D photonic bandgap in silica/air structures" Electron. Lett. **31** (22) (1995) 1941-1943.
11. H. Ebendorff-Heidepriem, P. Petropoulos, R. Moore, K. Frampton, D.J. Richardson and T.M. Monro "Fabrication and optical properties of lead silicate glass holey fibers", Journal of Non-Cryst. Solids **345-346** (2004) 293-296.
12. T.M. Monro, Y.D. West, D.W. Hewak, N.G.R. Broderick, D.J. Richardson,"Chalcogenide Holey Fibres", Electron. Lett., **36** (24) (2000) 1998-200.
13. T.M. Monro, D.J. Richardson, "Holey optical fibres: Fundamental properties and device applications", C.R. Phys.**4**, (2003) 175-186.
14. G. Renversez, B. Kuhlmey and R. McPhedran, "Dispersion management with microstructured optical fibers: ultraflattened chromatic dispersion with low losses", Opt. Lett., **28** (12) (2003) 989-991.
15. T.A. Birks, J.C. Knight, P.St.J. Russel, "Endlessly single mode photonic crystal fiber", Opt. Lett. **22** (1997) 961-963.
16. Y. Guimond, J.L. Adam, A.M. Jurdyc, H.L.Ma, J. Mugnier, B. Jacquier,"Optical properties of antimony-stabilised sulphide glasses doped with Dy and Er ions", Journal of Non-Cryst. Solids, **256&257** (1999) 378-382.
17. F. Smektala, C. Quémard, L. LeNeindre, J. Lucas, A. Barthélémy, C. De Angelis, "Chalcogenide glasses with large non-linear refractive indices," J. Non-Cryst. Solids **239** (1998) 139-42.
18. C. Quemard, F. Smektala, V. Couderc, A. Barthélémy, J. Lucas, "Chalcogenide glasses with high non linear optical properties for telecommunications," J. Phys. Chem. Solids 62 (2001) 1435-40 .
19. F. Smektala, J. Troles, P. Houizot, T. Jouan, G. Boudebs, S. Cherukulappurath, V. Couderc, P. A. Champert, "Third order non linearities of sulfur and selenide glasses at telecommunication wavelengths", SPIE **5451** (2004) 347-353.
20. G. Boudebs, S. Cherukulappurath, "Nonlinear optical measurements using a 4f coherent imaging system with phase objects", Phys. Rev. A **69** (5B) (2004).
21. E.M.Vogel, J. Am. Ceram. Soc. **72** (1989) 719-24.
22. L. Le Neindre, F. Smektala, K. Le Foulgoc, X. H. Zhang, J. Lucas, "Tellurium halide optical fibers" J. Non-Cryst. Solids **242** (1998) 99-103.
23. R. G.May, K.D. Bennett, "Ultra-low loss optical fiber characterization system development" Gov. Rep. Announce US Report Avail. NTIS. 90 (1990).
24. J.C. Knight,T.A Birks, P. St J. Russell, D.M. Atkin, "All-silica single mode optical fiber with photonic crystal cladding" Optics Lett. **21** (19) (1996) 1547-1549.
25. P. St J. Russell, "Photonic Crystal Fibers" Science **299** (5605) (2003) 358-362.
26. T.P. White, B.T. Kuhlmey, R.C. McPhedran, D.Maystre, G. Renversez, C. Martijn de Sterke, L.C. Botten, "Multipole method for microstructured optical fibers. I. Formulation.", Journal of the Optical Society of America B: Optical Physics **19**(10) (2002) 2322-2330.
27. B.T. Kuhlmley, T.P. White, G. Renversez, D.Maystre, L.C. Botten, C. Martijn de Sterke, R.C. McPhedran, "Multipole method for microstructured optical fibers. II. Implementation and results", Journal of the Optical Society of America B: Optical Physics **19**(10) (2002) 2331-2340.
28. G. Renversez, F. Bordas, B.T. Kuhlmey, "Second mode transition in microstructured optical fibers : determination of the critical geometrical parameter and study of the matrix refractive index and effects of cladding size", Optics Lett. **30** (11) (2005) 1264-6.
29. F. Bordas, L. Provino, G. Renversez, "High index microstructured optical fibers : losses and chromatic dispersion of fundamental mode and secon mode cut-off, comparison with silica », Proc. Journées Nationales d'Optique Guidée, Société Française d'Optique, (2004), Paris, France, 230-2.

13C5-3

Dispersion and nonlinear coefficient measurements in optical fibres using soliton-effect compression

T. N. Nguyen (1), T. Chartier (1), M. Thual (1), P. Rochard (1), L. Provino (2), A. Monteville (2), N. Traynor (2), V. Gaillard (3), C. Lupi (3), D. Leduc (3)

1: UMR FOTON, ENSSAT, 6 rue de Kerampont, 22300 Lannion, France; Thanh-Nam.Nguyen@enssat.fr

2: PERFOS, 11 rue de Broglie, 22300 Lannion, France, ntraynor@perfos.com

3 : Universite de Nantes, Nantes Atlantique Universites, IREENA, EA1770, Faculte des Sciences et des Techniques, 2 rue de la Houssiniere - BP 9208, Nantes, F-44000 France., Dominique.Leduc@univ-nantes.fr

Abstract *We present a novel and simple method to measure both the value of the second-order dispersion coefficient and the nonlinear coefficient in optical fibres. This method is based on the higher-order soliton-effect pulse compression phenomenon.*

Introduction

Nonlinear pulse propagation in optical fibres is influenced by both the group-velocity dispersion parameter D and the nonlinear coefficient γ [1]. The knowledge of both of these parameters is essential for a wide range of applications including optical transmission, nonlinear fibre optics or mode-locked fibre lasers. The recent development of highly-nonlinear holey fibres allows a broad range of values for these parameters to be covered (D, γ). Simple and efficient methods for the simultaneous measurement of both D and γ are therefore of great interest for the manufacturers or the users of these kinds of fibres. Some methods for the simultaneous measurement of D and γ are based on four-wave mixing [2,3] or modulation instabilities [4,5], but are only valid for low-dispersion fibres (around the zero-dispersion wavelength). The method proposed in Ref. [6] is valid for any value of the dispersion but requires non-conventional features like a frequency resolved optical gating technique and a numerical minimization algorithm.

In this paper we report a novel and simple method for the simultaneous measurement of the dispersion parameter D and the nonlinear coefficient γ for all types of fibres in the anomalous dispersion regime.

This method is based on higher-order soliton pulse compression effect and is an extension of the method proposed in Ref. [7].

Theory

In the anomalous dispersion regime, the soliton effect occurs as a result of the interplay between the group-velocity dispersion (GVD) and self-phase modulation. *N-th*-order solitons follow a periodic evolution pattern along the fibre such that they are periodically compressed by a factor that depends on the soliton order N given by [1]

$$N^2 = \frac{2\pi c \gamma P_0 T_0^2}{\lambda_0^2 D} \qquad (1)$$

where c is the speed of light in vacuum, T_0 the pulse duration, P_0 the input peak power and λ_0 the wavelength.

Previous work has shown that, for a given fibre length L, it is possible to find, by adjusting the peak power P_0, the lowest soliton order N that leads to the maximum compression of the output pulse [7,8]. In this case, the shape of the compressed output pulse depends only on the value of the soliton order N (depending itself on D and γ) and the relation between L and N is expressed by an empirical equation as follows [9]

$$L\left(\frac{\lambda_0}{\pi T_0}\right) D = \frac{0.32}{N} + \frac{1.1}{N^2} \qquad (2)$$

We propose a simple method, related to the shape of the autocorrelation trace of the compressed pulse, to extract the values of D and γ. The first parameter we measure is the compression factor F_a, defined as the ratio between the full width at half maximum of the initial and compressed pulses (see Fig. 1). The second parameter is the ratio R_a, defined as the ratio between the level of the main peak and the level of the secondary peaks of the compressed pulse (see Fig. 1). The last parameter is the peak power P_0 of the initial pulse. Similar to the work in Ref. [9], we have found approximate empirical relations to extract the values of D from the measured values of F_a, R_a with good accuracy.

$$L\left(\frac{\lambda_0}{\pi T_0}\right)^2 D \approx -\frac{3.224}{F_a^3} + \frac{3.373}{F_a^2} + \frac{1.774}{F_a} - 0.007 \qquad (3)$$

$$L\left(\frac{\lambda_0}{\pi T_0}\right)^2 D \approx -\frac{9.775}{R_a\sqrt{R_a}} + \frac{18.075}{R_a} - \frac{11.347}{\sqrt{R_a}} + 2.438 \qquad (4)$$

The method we propose works as follows. For a given length L of an anomalous dispersion fibre, by adjusting the power of a launched soliton pulse of duration T_0 at wavelength λ_0, we obtain the soliton order N that leads to the maximum pulse compression. Then, we measure the compression factor F_a (method A) and the ratio R_a (method B). According to equation (3), the value of F_a gives a value of dispersion which we shall call D_A and, according to equation (4), the value of R_a gives a value which we shall call D_B. In the ideal case (measurement without error) D_A and D_B are identical

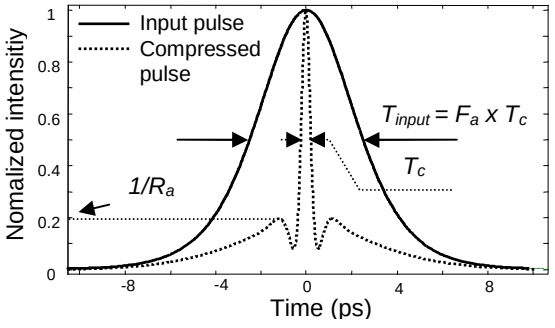

Fig. 1. Theoretical autocorrelation traces of an input pulse and a compressed pulse and definition of F_a and R_a

In fact, both values of D obtained with method A and method B can differ because they are obtained using approximate relations. Moreover, in these relations no impact of cubic dispersion, attenuation and higher-order nonlinearity are included.

Calculations of D_A and D_B when taking into account the effect of third order dispersion (β_3 = 0.1 ps^3/km), the effect of fibre loss (α = 0.2 dB/km), the effect of self steepening and stimulated Raman scattering (T_R = 3 fs) are carried out numerically. Fig. 2(a) shows the relative error between the theoretical values and the calculated

values of dispersion over a wide range of dispersion (from 0.2 ps/km/nm to 100 ps/km/nm). We note that these effects have a detrimental influence on the accuracy of the methods for the lower values of dispersion (D<1 ps/km/nm). We also note that the errors of each method are of the opposite sign. This can be explained as follows. When an output pulse is more compressed than in the ideal case (the measurement of F_a is over-estimated), the quality of the compressed pulse decreases [1] (the main peak is lower and the side-peaks are higher) and the measured value of R_a is under-estimated. Conversely, when an output pulse is less compressed than the ideal case, F_a is under-estimated and R_a over-estimated. By taking the average value of dispersion calculated from the two methods we have the final value of dispersion with an error less than 1% for D>1 ps/km/nm and less than 6% for D>0.5 ps/km/nm (see Fig. 2(b)).

Replacing the value of D in relation (2) allows us to determine N. Introducing the value of D and N in relation (1) allows us to find γ. The accuracy in the calculation of γ is on the same order than for D (Fig. 2(b)).

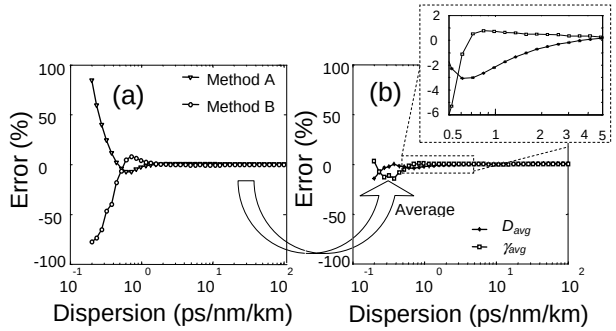

Fig.2. Errors in the calculation of D when the real effects are taken into account (a) and the averages (b)

Experiment and results

We performed dispersion and nonlinear coefficient measurements with a 30.5 m-long nonlinear holey fibre (NHF) fabricated by PERFOS. This fibre is a 5 ring silica NHF with an attenuation of 10 dB/km. The splice loss with standard single mode fibre (SMF) is around 1.5 dB. The experimental setup is shown in Fig. 3. The laser source is a passively-mode-locked tunable fibre laser working in soliton regime in the C band. Its repetition rate is 19.3 MHz. The mean power launched in the NHF is controlled with a power meter at the output of the 3 dB coupler.

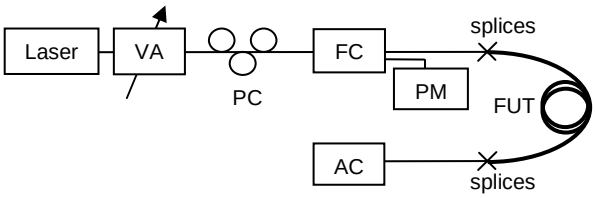

Fig. 3. Experimental set-up. VA: variable attenuator, PC: polarisation controller, FC: 3 dB fibre coupler, PM: power-meter, AC: Auto-correlator, FUT: fibre under test

We adjust the laser to have output pulses of T_0 = 6.24 ps at a wavelength λ_0 = 1555 nm. The peak power of pulses launched in the fibre for maximum compression is 3.8 W. From the autocorrelation traces we find F_a = 20.7 and R_a = 3.9. Therefore, the value of dispersion D and nonlinear coefficient γ are 112.5 ps/km/nm and 44 $W^{-1}km^{-1}$ respectively. Before comparing these results with other conventional methods, we also performed the measurement on a 304 m-long SMF. The wavelength is set to λ_0 = 1560 nm and the pulse duration is T_0 = 8.5 ps. The procedure of measurement is the same as above and we obtain P_0 = 13.5 W, F_a = 26.2, R_a = 3.8. The dispersion is found to be D = 17.2 ps/km/nm and the nonlinear coefficient γ = 1.4 $W^{-1}km^{-1}$.

The comparison between our results and the results obtained by conventional methods are summarized in table 1. The reference method used to measure the dispersion is the low coherence interferometry method [10]. The reference method used to measure the nonlinear coefficient is based on the measurement of the effective area of the optical fibre, knowing the nonlinear refractive index n_2 of silica [1].

Fibre	D_{Ref} (ps/km/nm)	D (ps/km/nm)	γ_{Ref} ($W^{-1}km^{-1}$)	γ ($W^{-1}km^{-1}$)
NHF	115	112.5	44.2	44
SMF	17.6	17.2	1.4	1.4

Table 1. Results of dispersion and nonlinear coefficient measurements of NHF at 1555 nm and SMF at 1560nm.

We find good agreement between our measured values and the values measured by other conventional methods, indicating that our method is valid and reliable.

Conclusions

We have proposed a novel and simple method for simultaneous measurement of both the dispersion and the nonlinear coefficient of optical fibres in the anomalous dispersion regime. This method is based on the soliton-compression effect in optical fibres and is reliable for dispersion values greater than 0.5 ps/km/nm. Experimental measurements were performed and have demonstrated the accuracy and reliability of the method.

Acknowledgements

This work is supported by the Conseil Regional de Bretagne and the European Union (Fonds Europeen de Developpement Regional).

References

1. G. P. Agrawal, Nonlinear Fiber Optics, 2nd Ed., Academic Press, New York, 1995.
2. P. S. Andre et al., Microwave Opt. Technol. Lett., **34** (2002), p. 305.
3. H. Chen, Optics Commun., **220** (2003), p. 331.
4. C. Mazzali et al., IEEE Photon. Technol. Lett., **11** (1999), p. 251.
5. J. Fatome et al., Opt. Fiber Technol., **12** (2006), p. 243.
6. L. P. Barry et al., Electron. Lett., **33** (1997), p. 707.
7. T. N. Nguyen et al., ECOC 2006, paper We3.P.12.
8. L. F. Mollenauer et al., Opt. Lett., **8** (1983), p.289.
9. E. M. Dianov et al, Sov. Tech. Phys. Lett., **12** (1986), p. 311.
10. P. L. Francois et al., J. Lightwave Technol. **7** (1989), p. 500.

Optical characterization of photonic crystal fibers by optical low coherence reflectometry and scanning near field optical microscopy

Virginie Gaillard[1], Loïc Lalouat[2], Cyril lupi[1], Dominique Leduc[1], Laurent Provino[3], Nicholas Traynor[3], Thanh Nam Nguyen[4], Thierry Chartier[4], Frédérique de Fornel[2] and Christian Boisrobert[1].

[1]Université de Nantes, Nantes Atlantique Universités, IREENA, EA1770, Faculté des Sciences et des Techniques, 2 rue de la Housinière - BP 9208, Nantes, F-44000 France;
[2]Institut Carnot de Bourgogne (ICB), Équipe Optique Champ Proche (OCP), 9 avenue Alain Savary, BP 47870, 21078 Dijon Cedex, France ;
[3]PERFOS, 11 rue Louis de Broglie, 22300 Lannion, France ;
[4]UMR FOTON, ENSSAT, 6, rue de Kerampont, 22300 Lannion, France.

ABSTRACT

We present the structure of photonic crystal fibers and give a characterization results in birefringence and chromatic dispersion using scanning near field optical microscopy and low coherence interferometry.

Keywords: Photonic Crystal Fiber, Chromatic Dispersion, Birefringence, Near-Field Optical Microscopy, Low-Coherence Interferometry

1. INTRODUCTION

Photonic Crystal Fibers (PCF) have very specific properties which are impossible to obtain with conventional fibers. The first samples were realized in the 90's and since they kept raising an increasing interest. For example, the hollow core fibers can guide high radiant power light beams without being damaged. One of these structures would be very useful in fiber optics telecommunication systems. Most of the research activities on the fabrication process are oriented toward high non linear coefficients and low chromatic dispersion. The fabrication of this kind of fibers requires precise characterization methods. In this paper, we show that low coherence interferometry (LCI) allows to measure the chromatic dispersion and the birefringence of photonic crystal fibers and we discuss about the precision of measurements.

Two types of fibers were characterized, which will be noted "hf107" and "hf146" thereafter. The fibers "hf107" were not connected. Light was coupled to the fiber using a lensed tip fiber (gradissimo[1] fiber) the focal length of which is approximately 37.5 μm. Two sections removed from the same fiber were studied. The "hf146" fiber samples were welded with high numerical aperture fibers (HNA) themselves welded with a single-mode fibers (SMF 28). Under these measurement conditions, the injection coupling into these fibers was effective. Indeed, losses between photonic crystal fibers and HNA fibers are from 1 to 4 dB depending on fibers and those between HNA fibers and SMF are of the order of 0.2 dB. Six of "hf146" fibers removed from six differents fibers have been characterized. The structures of all these "hf146" fibers, consist of hexagonal arrays of air-holes. Holes diameter d range from 0.76 μm to 1.57 μm and the distances between the centers of two adjacents holes Λ from 1.27 μm to 1.92 μm.

2. SCANNING NEAR FIEL OPTICAL MICROSCOPY

Figure 1 shows a simplified diagram of the Scanning Near field Optical Microscopy device (SNOM). The essential part of the set-up is the "probing head", represented in grey on the diagram. It is composed of a piezoelectric scanner, of a dither-tube (piezoelectric tube which permits the probe vibration) and finally of a probe (a bare optical fiber chemically attacked to obtain a tip form).

The topography of the sample surface can be obtained with the regulation itself controlled by a "shear-force" system. Figure 2 shows the principle diagram of this regulation. The farthest is the probe from the surface, the biggest is the amplitude of vibration of the probe. The regulation is carried out on this amplitude in order to record the topography of the sample. Then, to keep a scan of the surface with a constant distance, it is necessary to maintain constant the amplitude of vibration of the probe.

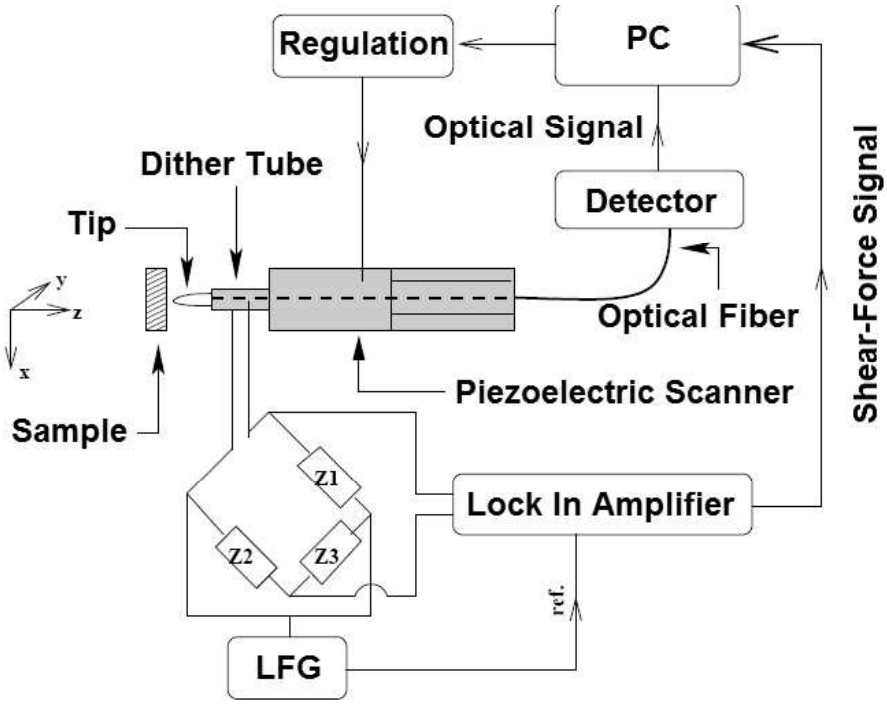

Figure 1. SNOM set-up.

An optical fiber used as a probe allows to record at the same time, the topography of the sample and a light distribution representation at the surface of the sample. In general, the distance between the probe and the surface ranges from 4 to 15 nm. An amplified spontaneous emission source is used to inject light into the PCF to record the light distribution on its end face.

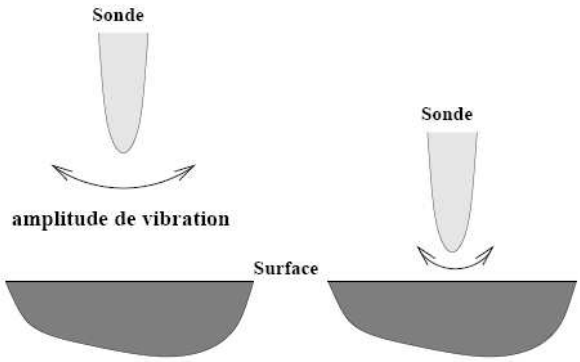

Figure 2. "Shear-force" regulation principle.

3. LOW COHERENCE REFLECTOMETRY

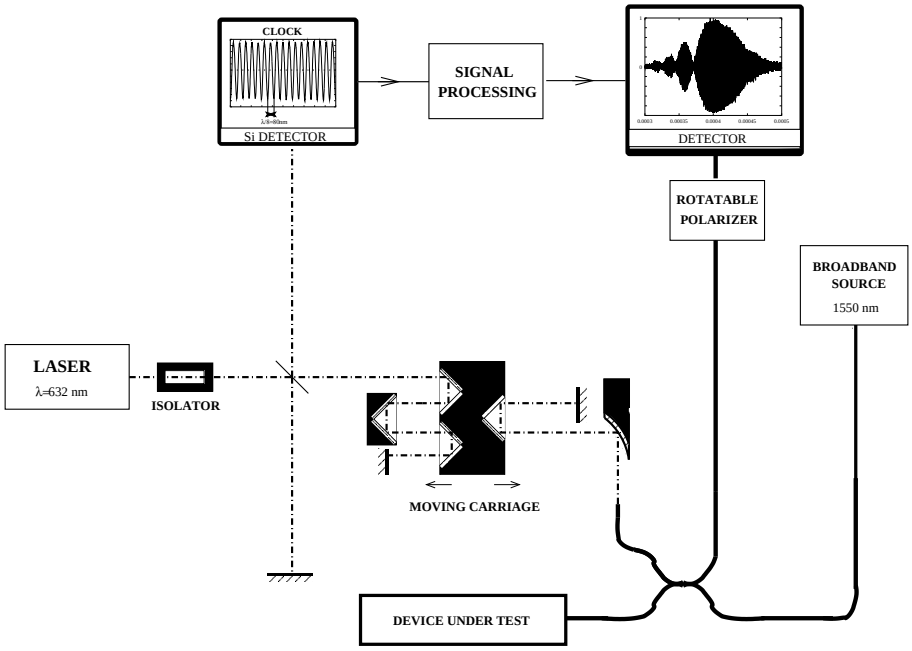

Figure 3. Optical low-coherence reflectometer.

The reflectometer used to characterize photonic crystal fibers is made up by two Michelson-interferometers (figure 3). The first one is almost entirely constituted of single-mode fibers and uses a broadband source emitting in the wavelength range 1525-1575 nm. The incident light is splitted by a "two-by-two" fiber coupler. One of his output fiber is connected to the sample under test and the other is used as a reference arm where the propagating wave is bent on a sliding corner cube reflector and oriented toward a fixed plane mirror. Interferences due to propagatives waves into differents arms of the fiber coupler are then obtained. The second Michelson-interferometer, in free space, is used as a fringe counter and samples the infrared interferogram every 80 nm ($\lambda_{\mathrm{He-Ne}}/8n_{\mathrm{air}}$). The intensity detected during the interferogram acquisition is :

$$I(x) = \int_{-\infty}^{+\infty} S(\sigma)\tilde{r}(\sigma)e^{-8i\pi n_{\mathrm{air}}\sigma x}d\sigma \tag{1}$$

where x is the displacement of the moving carriage, n_{air} the refraction index of the air, σ the wavenumber expressed in m^{-1}, $S(\sigma)$ the source spectral power density and $\tilde{r}(\sigma) = r(\sigma)e^{i\Phi(\sigma)}$ the complex amplitude reflection coefficient, with $\Phi(\sigma)$, the phase difference between the interfering waves.

Using a Fourier transform, the real and imaginary parts of the complex reflection coefficient can be easily calculated, which permit to obtain the amplitude reflection coefficient, the signal phase and its first and second derivatives. A rotating polarizer is placed in front of the infrared detector in order to select only one polarization mode which propagates along the waveguide.

The chromatic dispersion of the sample and the phaseshift ϕ_{samp} cause by this dispersion are bound by the relation :

$$D_\sigma = -\frac{\sigma^2}{4\pi\ell_{samp}c}\frac{d^2\phi_{samp}(\sigma)}{d\sigma^2} \tag{2}$$

where c is the light velocity. We have to withdraw the contributions of the fibers connected to the sample to determine $\phi_{samp}(\sigma)$ from the phase $\Phi(\sigma)$ given by (1). Two methods were used to do this depending on whether photonic crystal fibers were bare or connected to HNA fibers. In the first case, light was coupled through a

lensed tip fiber, the interferograms corresponding to rear and front faces of the sample were recorded. The phase difference produced by the sample was then obtained by substracting the rear and front phase calculated from these interferograms. In the second case, the length of the HNA fibers was not known accurately, so two acquisitions were recorded, one before and one after a short length of fiber sample had been cut. Once the phase shifts were withdrawn during the two acquisitions we obtained the phase shift caused by the short cut sample only.

When the fiber birefringence is high enough, beat lobes can be observed in the reflection coefficient amplitude.[2] Indeed, in this case, there are two interferograms corresponding to the two orthogonal polarizations, separated by the distance $\Delta n\,\ell_{samp}$ where Δn is the birefringence and ℓ_{samp} the sample length. The intensity received by the detector can be expressed : $I(x) = I_0(x) + I_0(x - 2\Delta n\ell_{samp})$ and in the Fourier domain, $I(\sigma) = I_0(\sigma)\left[1 + \exp\left(8i\pi\Delta n\ell_{samp}\sigma\right)\right]$ with the modulus : $\|I(\sigma)\| = \|I_0(\sigma)\|\cos\left(4\pi\Delta n\ell_{samp}\sigma\right)$. The birefringence of the sample can then be written :

$$\Delta n = \frac{1}{2\,\ell_{samp}\,\Delta\sigma} \tag{3}$$

where $\Delta\sigma$ is the beat period in the spectrum. This relation can be directly used for bare fibers. For the others, the birefringence has been measured in two steps, the same way we already used and described for the chromatic dispersion measurement. The beat period has been measured before ($\Delta\sigma_1$) and after ($\Delta\sigma_2$) a piece of fiber was cut. The birefringence can then be expressed by :

$$\Delta n = \frac{(\Delta\sigma_2 - \Delta\sigma_1)}{2\,\Delta\sigma_1\,\Delta\sigma_2\,\Delta\ell} \tag{4}$$

where $\Delta\ell$ is the length of the cut piece of fiber.

The orientations of eigen axis of the fibers, noted $0°$ and $90°$ thereafter, correspond experimentally to the directions of the polarizer which reduce the beat lobes down to zero. We then have to rotate and adjust the polarizer axis along the two eigen axis to measure the chromatic dispersions corresponding to $0°$ and $90°$. We measure the birefringence when the beat lobes amplitudes are maximum i.e. the polarizer axis tilt angle is $45°$.

4. RESULTS

4.1. Photonic crystal fiber structure and birefringence

A fiber sample referenced "hf107" was analysed using Scanning Near Field Optical Microcopy. We coupled a broad spectrum light source to the sample under test (between 1525 and 1575 nm). The light intensity detected by the probe was filtered through a band pass filter centered on 1550 nm. We obtained a topography of the fiber facet surface from the servo controller even when the probe dropped into the holes by more than 1 μm (cf figure 4(a)).

On the image presented on figure 4(b), we may notice the presence of a gaussian shape on the core location. In order to get a better knowledge of the gaussian parameters, we proceeded to two cuts, one along the fast axis of the scan (figure 5(a)), the other along the slow axis (figure 5(b)). The two gaussian "1/e" widths are 1.9 and 1.6 μm and their respective "foot" widths are 3 and 2.5 μm. A rectangular scan slightly below the cavity showed that the maxima of signals detected from the gaussian and from the photonic crystal were in a ratio of 10.

These results are in good agreement with the simulations predicting a mode diameter of 1.74 μm. A small anisotropy in the mode shape may be observed which implies a birefringence of the fiber. This was confirmed by LCI measurements : two samples with L_1=53.4 cm and L_2=93.4 cm length were characterized. The amplitude reflection coefficient are plotted on figure 6. The beat lobes are respectively of the order of 10 nm and 5.8 nm, which lead, using relation (3), to a birefringence of $(2.208 \pm 0.004)\times10^{-4}$ at 1550 nm.

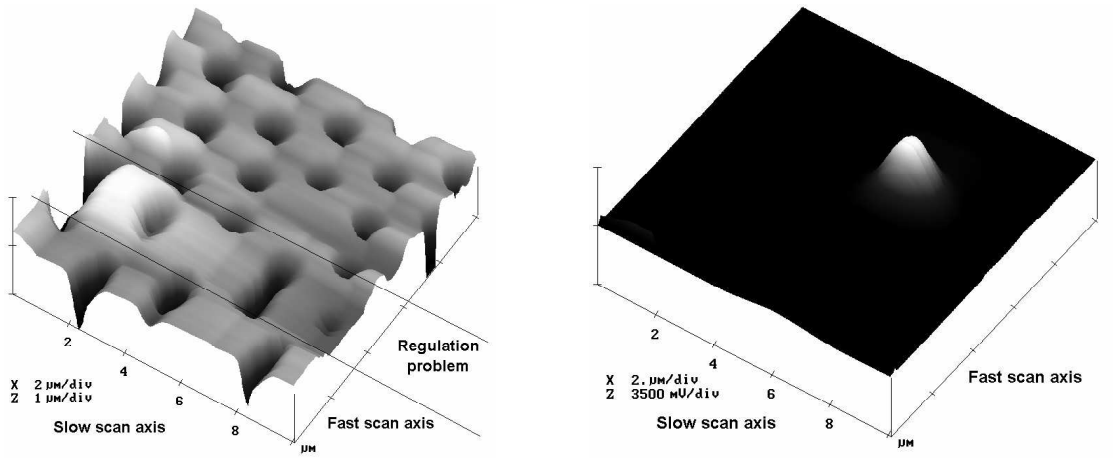

(a) (b)

Figure 4. 10 μm topographic (a) and optical (b) scans.

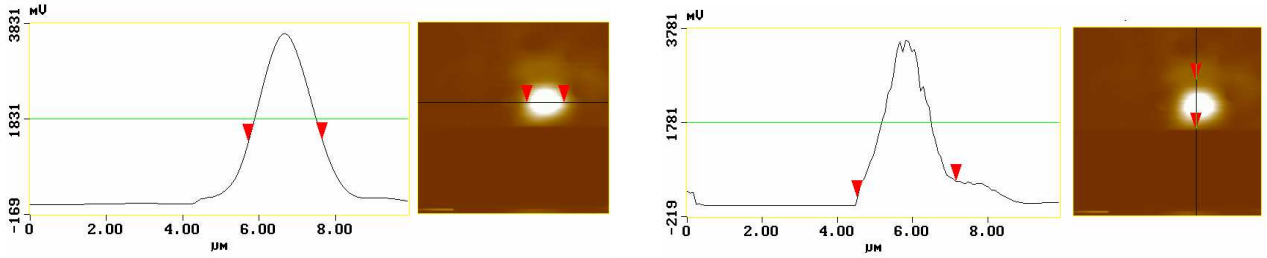

(a) (b)

Figure 5. Gaussian light distribution along fast (a) and slow (b) axis scans.

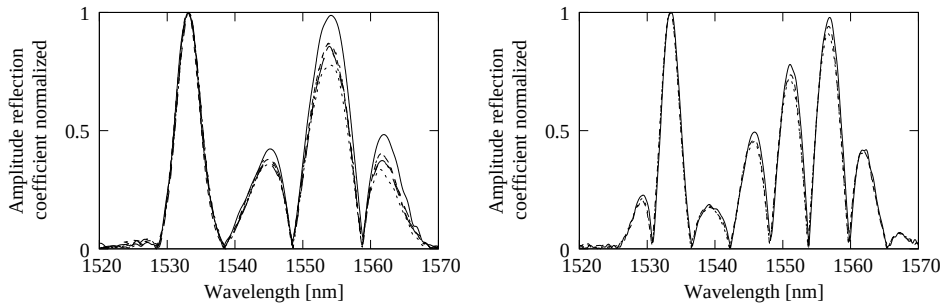

(a) (b)

Figure 6. Amplitude reflection coefficient of L_1 and L_2 fibers end faces.

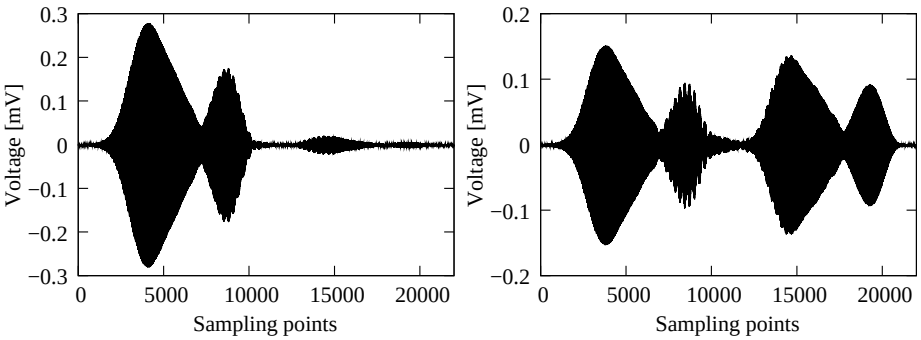

(a) Interferogram obtained for the angle 0° (b) Interferogram obtained for the angle 45°

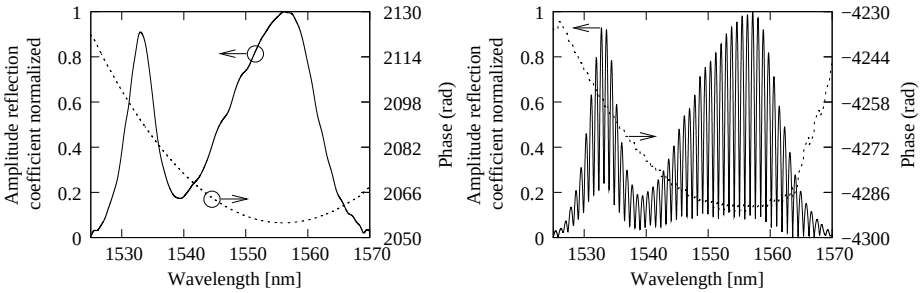

(c) Reflection coefficient obtained for the angle 0° (d) Reflection coefficient obtained for the angle 45°

Figure 7. Interferograms and reflection coefficients of "hf146" fiber for two states of polarization.

4.2. Birefringence and chromatic dispersion vs fiber structure

The interferograms obtained on a "hf146" sample corresponding to 0° and 45° polarization are presented on figures 7(a) and (b). For the latter, the interferograms corresponding to the two eigenstates of polarization can be detected but only one of them remains for the angle 0°. These phenomenons are shown in figures 7(c) and (d), where in the second one (45°), the beat lobes are observable. The beat lobe period is much smaller in the case of the "hf146" compared to the "hf107" for the same lengths of samples, which implies that "hf146" has a higher birefringence than "hf107". Indeed, the birefringence is $(1.45\pm0.02)\times10^{-3}$ at 1550 nm.

Figure 8 shows calculated values of birefringence for differents "hf146" type photonic crystal fibers. The birefringence increases with the ratio d/Λ. For d/Λ=0.6, the birefringence is equal to $7.42.10^{-4}$. It is of the order of 1.5 10^{-3} for the other fibers. The absolute uncertainties on these measurements are of the order of 1.10^{-5}. The sources of uncertainties are the errors on measurements of fiber lengths and beat lobes period. In our case, the latter predominates. The error on the length is of the order of 0.5 mm, for 30 cm long samples which gives an uncertainty on the birefringence of 10^{-6}. The error on the wavelength is about 10 picometers,[3] which corresponds to an error of 4.10^{-6} μm^{-1} on the wavenumber. This leads to an uncertainty on the birefringence of the order of 10^{-5}, since we consider approximately fifty beat periods.

The measurement resolution is limited by the source spectral width. Two oscillations in the reflection coefficient amplitude are required to determine the birefringence. Then, the beat lobe period must be at least of 20 nm. Since the longest sample we can measure with the reflectometer is about 1 m, the smallest birefringence which can be measured is about 6.10^{-5}.

The chromatic dispersion of the differents fibers were measured using methods described in section 3. Series of ten measurements for the three states of polarization were recorded. As the chromatic dispersion is calculated using Fourier transform and polynomial fitting, it is difficult to determine precisely how the uncertainties propagates through the whole numerical process. However, LCI has already been proved to give precise measurements,[3,4] and then it is possible to estimate the error from the range of measurements. In this case, the

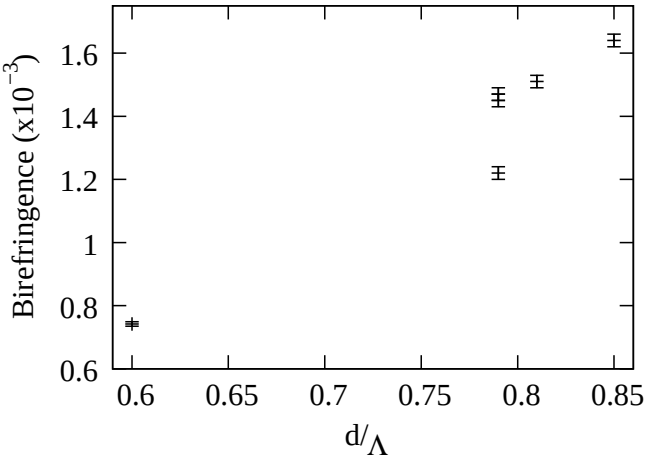

Figure 8. Birefringence obtained for differents holey fiber diameters.

maximum deviation from the mean value is about 7 ps/nm/km. Figure 9 shows the mean chromatic dispersion at 1550 nm of differents fibers for the eigenstates of polarization. From this graph, we can outline several points. First of all, all the fibers we characterized have strong dispersion ($D_\sigma > 100$ ps/km/nm) except the one with a d/Λ ratio equal to 0.6 which has a weak and negative dispersion about -17.5 ps/nm/km and -15.8 ps/nm/km respectively for 0° and 90°. We must notice that these different fibers have also been measured by two others methods based on higher-order soliton pulse compression effect[5,6] and the chromatic dispersions then obtained are in good accordance with our values. For example, the chromatic dispersion obtained by the compression method[6] for a 92 μm diameter fiber (d/Λ=0.79) is about 112.5 ps/nm/km, whereas with LCI technique, it is about 113.6 ps/nm/km and 106.3 ps/nm/km for the two eigen axis of polarization. Furthermore, the fiber birefringence is related to the difference between the dispersions along the two eigen axis of the fiber. The maximum value for this difference is 10.4 ps/nm/km and drops to 1.4 ps/nm/km for the 0.6 d/Λ ratio fiber. Finally, we can observe an increase of the dispersion with the d/Λ ratio, which agrees with the simulations (triangles on figure 9).

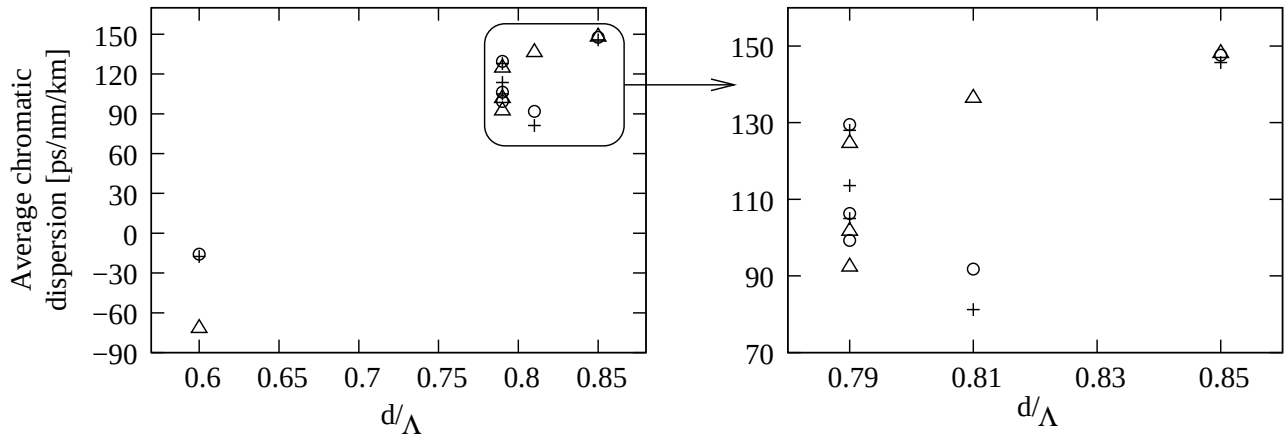

Figure 9. Chromatic dispersions for 1550 nm: (+) angle 0°, (○) angle 90° and (△) simulations.

The slope of the curve of dispersion is also an important parameter in telecommunication applications. This parameter has been calculated from the curves of dispersion and the values that are derived are shown in figure 10. The slopes of dispersion of the differents fibers are in general around 0.25 ps/nm^2/km, with an uncertainty of

2×10^{-2} ps/nm^2/km. The differents remarks done about the chromatic dispersion remain valid for the slope. There is a difference between the slopes corresponding to the two eigen axis of the fiber and an increase of the slope with the d/Λ ratio. For d/Λ=0.6, the slope of dispersion is weak and negative : -0.046$\pm$0.003 ps/nm^2/km for one direction of polarization and -0.042$\pm$0.002 ps/nm^2/km for the other.

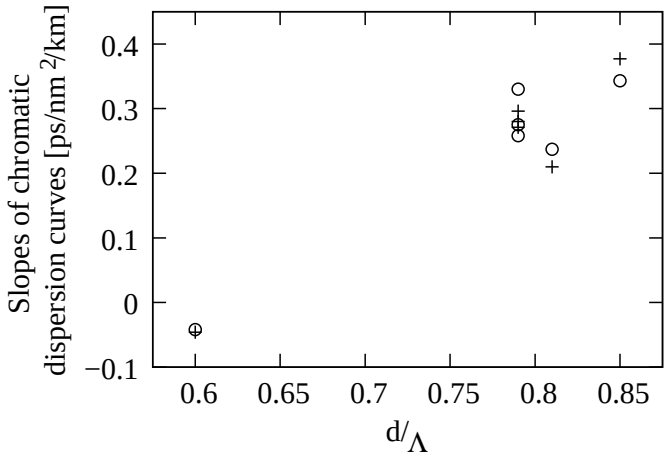

Figure 10. Slopes of chromatic dispersion curves obtained for differents holey fiber diameters : (+) angle 0°, (∘) angle 90°.

5. CONCLUSION

We have shown that the birefringence of photonic crystal fibers can be characterized by LCI within 10^{-5} absolute accuracy. Using a 40 nm spectral with light source, birefringence greater than 6.10^{-5} can be detected on 1 m long fiber samples. We can also use LCI to characterize dispersion and dispersion slopes of these fibers with respective accuracies of 7 ps/nm/km and 2×10^{-2} ps/nm^2/km. From the analysis of the microstructured fibers optical properties and their variations with the d/Λ ratios, we have shown that the chromatic dispersion and its slope would increase with the ratio d/Λ. Thus, the chromatic dispersion of the 0.6 d/Λ ratio fiber is close to those of a single mode fiber in absolute value and its slope is weak. This fiber could then be interesting for telecommunications.

REFERENCES

1. P. Chanclou, H. Ramanitra, P. Gravey, L. Bonnel, and M. Thual, "Design and performance of expanded mode fiber using micro-optic," *IEEE Journal of Lightwave Technology* **20**, pp. 808–814, 2002.
2. C. Palavicini, Y. Jaouën, G. Debarge, E. Kerrinckx, Y. Quiquempois, M. Douay, C. Lepers, A.-F. Obaton, and G. Melin, "Phase-sensitive optical low-coherence reflectometry technique applied to the characterization of photonic crystal fiber properties," *Optics Letters* **30**, pp. 361–363, Feb. 2005.
3. D. Leduc, X. Chapeleau, C. Lupi, R. Le Ny, and C. Boisrobert, "Accurate low-coherence interferometric relative group delay and reflectance measurements; characterization of a free space optics multiplexer/demultiplexer," *Journal of Optics A : Pure and Applied Optics* **5**, pp. 124–128, 2003.
4. A. H. Rose, C. M. Wang, and S. D. Dyer, "Round robin for optical fiber bragg grating metrology," *Journal of Research of NIST* **105**(6), pp. 839–866, 2000.
5. T. Nguyen, T. Chartier, M. Thual, P. Besnard, L. Provino, A. Monteville, and N. Traynor, "Higher-order soliton-effect pulse compression in a non-linear holey fibre. Application to second-order dispersion measurement," *ECOC'2006,Cannes* , p. 12, sept 2006.
6. T. Nguyen, T. Chartier, M. Thual, P. Besnard, L. Provino, A. Monteville, and N. Traynor, "Une nouvelle méthode pour mesurer simultanément la dispersion et le coefficient non-linéaire de fibres optiques à dispersions positives," *JNOG 2006,Metz, France* , nov 2006.